Natural Product Reports

ROYAL SOCIETY OF CHEMISTRY

REVIEW

Published on 12 August 2026

Cite this: DOI: 10.1039/d6np00044d

Pyrrocidines and hirsutellones: distinctive fungal polyketide alkaloid hybrids with intriguing therapeutic applications: a comprehensive update

Mohamed A. Tammam, [a] Islam El-Awaad, [bcd] Adnane Aouidate,[e] Reham Hassan Mekky [f] and Amr El-Demerdash [*ghi]

Received 10th April 2026

DOI: 10.1039/d6np00044d

rsc.li/npr

Covering: 2005–2025

Pyrrocidines and hirsutellones are a fascinating class of fungal natural products that possess an intricate chemical structure characterized by a distinctive macrocyclic ring fused to a decahydrofluorene core. Known for their complex architectures as PKS-NRPS hybrids, these metabolites are isolated from various fungi and have attracted significant attention due to their potent pharmacological properties, including antimicrobial, antifungal, and anticancer effects. This review article aims to shed light on the structural diversities of 52 fungal-derived pyrrocidines and hirsutellones reported over the period of 2005–2025, providing insights into their chemistry, biosynthetic origins, pharmacokinetic profiles, and structure–activity relationships (SARs). Furthermore, we critically evaluate their promising therapeutic potential, highlighting the opportunities they present for modern drug discovery and development.

[a]Department of Biochemistry, Faculty of Agriculture, Fayoum University, Fayoum 63514, Egypt

[b]Institute of Pharmaceutical Biology, Technische Universität Braunschweig, Mendelssohnstraße 1, 38106 Braunschweig, Germany

[c]Center of Pharmaceutical Engineering (PVZ), Technische Universität Braunschweig, Franz-Liszt-Straße 35 A, Braunschweig, 38106, Germany

[d]Department of Pharmacognosy, Faculty of Pharmacy, Assiut University, Assiut 71526, Egypt

[e]School of Applied Sciences-Ait Melloul, Ibn Zohr University, Agadir, Morocco

[f]Department of Pharmacognosy, Faculty of Pharmacy, Egyptian Russian University, Cairo-Suez Road, Badr City, Cairo, 11829, Egypt

[g]School of Chemistry, Pharmacy and Pharmacology, University of East Anglia, Norwich Research Park, Norwich NR4 7TJ, UK. E-mail: A.Eldemerdash@uea.ac.uk; a_eldemerdash@mans.edu.eg

[h]Chemistry Department, Faculty of Sciences, Mansoura University, Mansoura 35516, Egypt

[i]Center for Microbial Interactions, Norwich Research Park, Norwich NR4 7UG, UK

1. Introduction

Natural products have historically been a cornerstone of drug discovery and continue to serve as key contributors to modern medicinal chemistry.[1,2] These compounds are biosynthesized in several matrices, such as plants, microorganisms, fungi, and marine species.[3–5] They have developed over millions of years to interact with biological macromolecules in a selective and efficient manner. Hence, these natural products exhibit a diverse array of structures, stereochemical intricacies and biological specificities that are difficult to be produced solely through synthetic approaches.[6] The distinctive chemical diversity accounts for the substantial proportion of approved

medications derived from natural products, particularly in domains of infectious diseases, oncology, and immunology.[7]

Among natural resources, microorganisms, including fungi and bacteria, are prolific factors of natural products, characterized by highly evolved biosynthetic pathways, resulting in the isolation of several natural products with a wide array of structural diversity and potent biological activities.[2,8] Furthermore, fungi are distinguished by an exceptional capacity for secondary metabolism, emphasized by highly sophisticated biosynthetic environments. Central to this capability are polyketide synthases (PKSs), nonribosomal peptide synthetases (NRPSs), and hybrid PKS-NRPS systems, which function as modular enzymatic assembly lines.[9] These systems operate with remarkable precision, allowing fungi to construct complex carbon frameworks enriched with multiple stereocenters with functional groups. Unlike conventional synthetic routes, fungal biosynthesis integrates chain elongation, cyclization, and stereochemical control into a single coordinated process.

As a result, fungal natural products encompass a wide spectrum of compound classes, including polyketides, alkaloids, peptides, terpenoids, and isocoumarins, many of which possess structural features that have no close counterparts in synthetic compound libraries.[3,9,10] In this context, fungi have yielded numerous clinically important secondary metabolites, including anti-inflammatory compounds, like cordycepin and gliotoxin,[11,12] cholesterol-lowering agents, including lovastatin and pravastatin,[13] anticancer drugs, such as taxol,[14] immunosuppressive agents, including cyclosporine A and mycophenolic acid,[15] and antibiotics, such as penicillin and cephalosporins.[16]

As part of our ongoing investigation into biologically active natural products, with particular emphasis on pharmacologically relevant fungal-derived natural products (FNPs),[2,9,17–19] herein, we provide a comprehensive and up-to-date literature review of pyrrocidines and hirsutellones exclusively isolated from diverse fungal strains.

Despite the growing body of literature addressing fungal secondary metabolites and PKS-NRPS-derived metabolites, existing reviews have largely approached pyrrocidines and hirsutellones either as individual examples within broader discussions of fungal alkaloids or as illustrative cases in biosynthetic and synthetic studies. Early comprehensive reviews have focused on the mechanistic and synthetic logic of hybrid PKS-NRPS pathways and have included selected hirsutellone derivatives among other complex fungal metabolites, without aiming to consolidate this scaffold as a distinct chemical family or to analyse its biological evolution over time.[20]

Indeed, the complex architectural traits of these PKS-NRPS hybrids have inspired landmark total syntheses by prominent

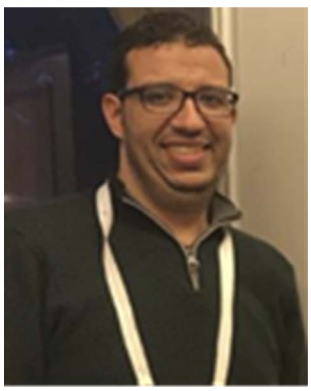

Mohamed A. Tammam

Dr Mohamed A. Tammam earned his BSc degree in soil and water science (2008) and MSc degree in biochemistry (2013) from the Fayoum University, Egypt. In 2020, he completed his PhD degree in Pharmacy with distinction from the National and Kapodistrian University of Athens (NKUA), studying Red Sea marine secondary metabolites under Prof. Vassilios Roussis and Prof. Efstathia Ioannou. After serving as an Assistant Professor in the Fayoum University's Faculty of Agriculture, he initiated his postdoctoral research at the NKUA in May 2021. His work focuses on the isolation, structural elucidation, and bioactivity evaluation of secondary metabolites derived from marine macro- and microorganisms.

Islam El-Awaad

Dr Islam El-Awaad is a Lecturer at the Faculty of Pharmacy, Assiut University, Egypt. He received his PhD degree from the Institute of Pharmaceutical Biology at the TU Braunschweig, Germany, where his research focused on the identification and engineering of the cytochrome P450 enzymes. He subsequently completed a three-year postdoctoral stay at the Institute of Biotechnology, RWTH Aachen University, Germany, gaining experience in the directed evolution of enzymes and microgel-based immobilization of heme-thiolate proteins. Since 2022, he has held a Group Leader position at the TU Braunschweig, where his research focuses on elucidating natural product biosynthetic pathways and advancing protein engineering for synthetic biology applications.

Adnane Aouidate

Dr Adnane Aouidate earned his BSc (2009) and MSc (2014) degrees in organic and natural product chemistry from the Moulay Ismail University, Morocco, receiving the Best Student awards for both. In 2019, he completed his PhD degree in Computer-Aided Drug Design at the UMI, utilizing the 3D-QSAR, molecular docking, and ADMET strategies for kinase inhibitor discovery. He undertook postdoctoral fellowships at both the Shenzhen Institute of Advanced Technology (Chinese Academy of Sciences) and the Institute of Organic and Analytical Chemistry (ICOA) in France. In early 2023, Dr Aouidate was appointed as an Assistant Professor at the School of Applied Sciences of Ait Melloul, Ibn Zohr University, Morocco.

synthetic groups, including Nicolaou and Sorensen. These pioneering synthetic strategies not only showcased brilliant approaches to stereochemical control and macrocyclization but also were pivotal in definitively confirming or revising early structural assignments. However, while these synthetic milestones are deeply elegant, a comprehensive evaluation of their evolving methodologies warrants dedicated discussion elsewhere.[21–25]

More recent surveys have expanded the coverage of fungal alkaloids and natural products across terrestrial and marine sources; nevertheless, pyrrocidines and hirsutellones are typically reported as isolated entries within extensive compound inventories, with limited comparative analysis of their structural diversification, structure–activity relationships, or biosynthetic variations.[26] Notably, no dedicated review has systematically integrated pyrrocidine and hirsutellone derivatives reported since 2005, despite the steady expansion of this family and the accumulation of biological data revealing their structure-dependent selectivity. The absence of a focused synthesis linking chemical diversity, biological activity, and biosynthetic context has limited a holistic understanding of these metabolites as a coherent and evolving class of fungal natural products. To address this gap, this work provides a comprehensive and up-to-date survey covering the period from 2005 to 2025, focusing on the chemical diversity and biological activities of pyrrocidines and hirsutellones isolated from fungal sources. This review systematically catalogues a total of fifty-two pyrrocidine and hirsutellone derivatives, detailing their distribution across a wide array of fungal genera, along with the pharmacological activities, biosynthesis, pharmacokinetics and druglikeness properties associated with these fungal-derived metabolites.

2. Recent advances in pyrrocidine and hirsutellone biosynthesis

Pyrrocidines, hirsutellones, and structurally related analogues such as the GKK1032 s share a characteristic molecular architecture, comprising a fused [6.5.6] tricarbocyclic decahydrofluorene core connected through an aryl-ether bridge to a highly strained 13-membered paracyclophane macrocycle. Over the past two decades, substantial efforts have been devoted to understanding the complex biosynthesis of paracyclophane–decahydrofluorene-containing natural products. First attempts were made by Oikawa using *Penicillium* sp. 1032GKK.[27] Multiple feeding experiments with an isotope-labelled precursor were performed to deduce the biosynthetic origins of GKK1032A_2 (**12**). The incorporation patterns of [1-^{13}C]-L-tyrosine, [*S*-$^{13}CH_3$]-L-methionine, and [1,2-^{13}C]acetate in **12** provided initial evidence for the involvement of a fungal hybrid polyketide synthase-nonribosomal peptide synthetase (PKS-NRPS) in the biosynthesis of 1032GKKs. [1-^{13}C,$^{2}H_3$] acetate feeding experiments indicated that acetyl-CoA serves as the starter unit, as inferred from the double deuteration of the terminal vinyl group in **12** (Scheme 1).

Oikawa[27] concluded that a highly reducing PKS domain catalyses the stepwise condensation of an acetyl-CoA starter with eight malonyl-CoA extender units. During chain elongation, five *S*-adenosyl methionine (SAM) units would add methyl groups to the growing chain. The polyketide chain is subsequently coupled to L-tyrosine *via* an NRPS domain, releasing a linear tyrosine-nonaketide aldehyde (**B1**) that subsequently undergoes intramolecular condensation, yielding the 3-pyrrolin-2-one (**B2**) key intermediate (Scheme 2). Various hypotheses have been postulated to explain the subsequent cyclization steps leading to the formation of **B2** from **12**. The

Reham Hassan Mekky

Dr Reham Hassan Mekky is an Associate Professor of Pharmacognosy at the Egyptian Russian University (ERU). She received her BSc and MSc degrees with distinction from the Ain Shams University and earned a joint PhD degree from Cairo University and the University of Granada through the Erasmus Mundus program. She has published 41 SCOPUS-indexed papers focused on pharmacognosy, natural product chemistry, traditional medicine, functional foods, and marine natural products. Dr Mekky is the Co-Founder and Associate Editor of the ERU Research Journal *and an active member of professional organizations, including the Society of Chemical Industry and the Italo-Latin American Society of Ethnomedicine.*

Amr El-Demerdash

Dr Amr El-Demerdash is an Assistant Professor and Junior Group Leader in Chemical Biology at the University of East Anglia, UK, and an Associate Professor at Mansoura University, Egypt. He holds a PhD degree in Organic Chemistry from the CNRS-ICSN, the University of Paris-Saclay, and has completed his postdoctoral training at Sorbonne University and the John Innes Centre. In August 2024, he established his research group at the UEA. His laboratory focuses on natural product-based drug discovery, combining isolation, structural elucidation, biomimetic total synthesis, biocatalysis, and biosynthetic pathway investigation to identify and develop novel pharmacologically active compounds from natural sources.

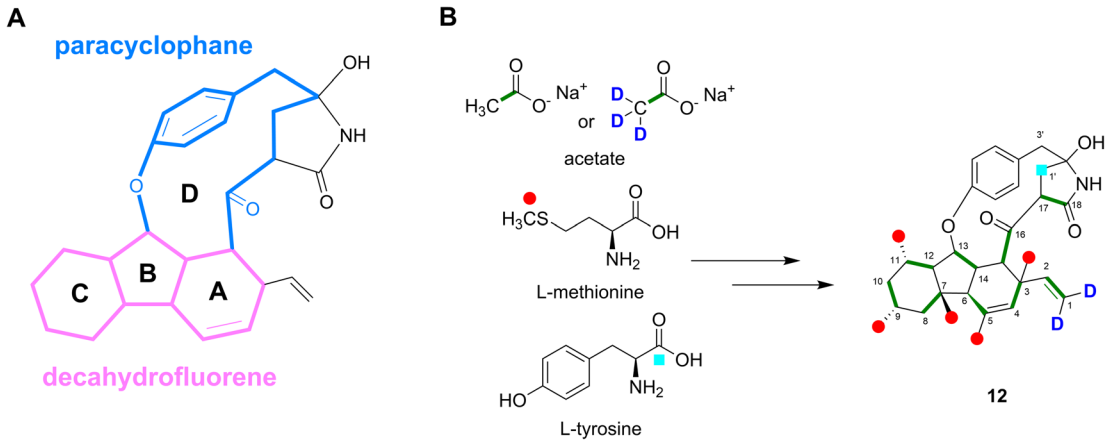

Scheme 1 (A) General structure of the paracyclophane–decahydrofluorene natural products. (B) Isotope-labelled profile of **12** based on the precursor incorporation studies by Oikawa.[27]

mechanistic basis underlying these hypotheses has been thoroughly reviewed by Li *et al.*[20]

A similar approach was employed by Ear *et al.* to investigate the origin of the oxygen atom in the ether bond of pyrrocidines.[28] Isotope-feeding experiments were performed using the maize endophyte *Acremonium zeae* NRRL 13540 (syn. *Sarocladium zeae*). Analysing the isotope incorporation pattern in pyrrocidines A (**34**) and B (**13**) upon feeding doubly labelled L-tyrosine ($^{18}O/^{13}C$) provided experimental evidence for the involvement of tyrosine phenolic oxygen in the formation of the strained paracyclophane ring D. Three plausible mechanisms have been proposed for the initiation of the intramolecular cyclization reactions of the linear polyketide **B3**, all leading to the formation of rings C and D with a concomitant rearrangement of the side-chain double bonds to yield **B4** (Scheme 3). The first mechanism involves hydroxylation at C1 by allylic oxidation, followed by dehydration and double bond rearrangement, affording ring C. Intramolecular attack of the tyrosine phenolic oxygen on the resulting carbocation would result in the formation of the paracyclophane ring D (Scheme 3a). The second pathway may be initiated by the epoxidation of the C12–C13 double bond, followed by deprotonation at C1, leading to double bond rearrangement and ring C formation. A dehydration reaction leads to the same carbocation species described in the previous pathway (Scheme 3b). The third possibility involves a phenolic radical that undergoes concerted cyclization to afford the paracyclophane ring D and cyclohexane ring C, resulting in the rearrangement of the double bonds, aided by allylic hydrogen abstraction at C1 (Scheme 3c).

The intermediates **B6**, **B7**, and **B4**, generated from the initial cyclization and double-bond rearrangement of the linear pyrrolidones **B5**, **B2**, and **B3**, have been proposed to undergo an intramolecular Diels–Alder (IMDA) reaction to afford the decahydrofluorene ring system characteristic of hirsutellones,

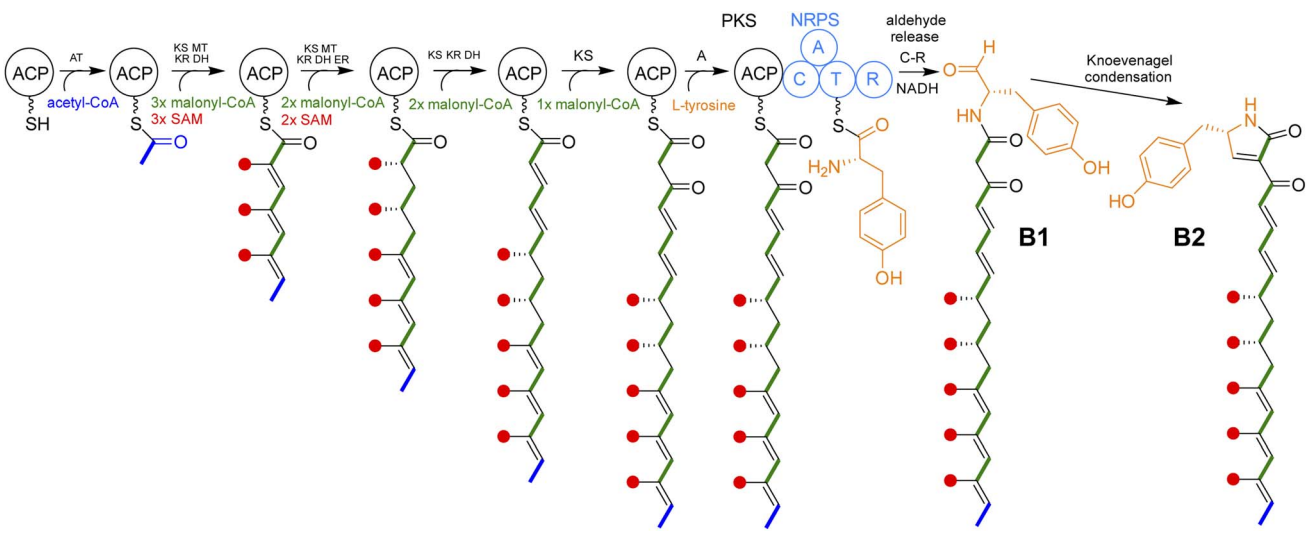

Scheme 2 Stepwise assembly of a methyl-decorated linear nonaketide chain by PKS, followed by the incorporation of L-tyrosine by NRPS. The released aldehyde, **B1**, undergoes intramolecular condensation to give **B2**. Adapted from Li *et al.*[20]

GKK1032 s, and pyrrocidines **B8–B11** (Scheme 4). The IMDA reaction may proceed *via endo* or *exo* transition states, leading to diastereomeric products with either *trans*- or *cis*-fused A/B ring junctions, respectively. Studies aiming at the synthesis of the decahydrofluorene core of hirsutellone B (**36**) have demonstrated that the *endo* IMDA reaction is chemically favoured, suggesting that the formation of *exo* analogues may require enzymatic catalysis.[21,25]

The precise enzymatic background of the cyclization steps remained obscure until Ohashi *et al.*[22] sequenced the genome of *A. zeae* (syn. *S. zeae*). A biosynthetic gene cluster (BGC), named *pyd*, was selected for biochemical investigation as it contained PydB sharing ~40% identity with the Diels–Alderases involved in the biosynthesis of decalin natural products. PydB was initially thought to be responsible for directing the *exo* IMDA reaction, but subsequent biochemical characterization showed that this was not the case. Systematic heterologous co-expression of different gene combinations from the *pyd* cluster in *Aspergillus nidulans* ΔEMΔST, followed by LC-MS and NMR analyses of the produced metabolites, was performed. The initial co-expression of PydA (PKS-NRPS), PydC (*trans*-ER), and PydG (α/β-hydrolase) gave rise to three shunt products, **B12–B14**, related to the expected linear 3-pyrrolin-2-one nonaketide intermediate **B3** (Scheme 5), indicating that additional enzymes are needed to proceed with the biosynthesis. Additional co-expression of the putative Diels–Alderases PydB (LLP) and PydE (MDR) did not result in any additional products. Sequence comparisons with homologous fungal BGCs from *Phialocephala scopiformis* and *Penicillium citrinum* DSM 1997 led to the identification of hypothetical proteins PydX and PydZ as conserved members of BGCs potentially involved in pyrrocidine biosynthesis. Upon co-expression of all seven proteins (PydA/C/G/B/E/X/Z), a decrease in the production of shunt products was observed. Additionally, pyrrocidine D **B15**, and not the anticipated **13**, was produced. Compound **13** possesses a cis A/B ring system arising from an *exo* IMDA reaction, while **B15** originates from an *endo* IMDA reaction and was not observed by the authors as a natural metabolite in *A. zeae*. The presence of four proteins (PydB/E/X/Z) was deemed essential for the reaction to proceed, as the removal of any of them led to the loss of **B15** production. It was proposed that those four proteins assemble into a functional complex to produce **B4** from **B3**, with the

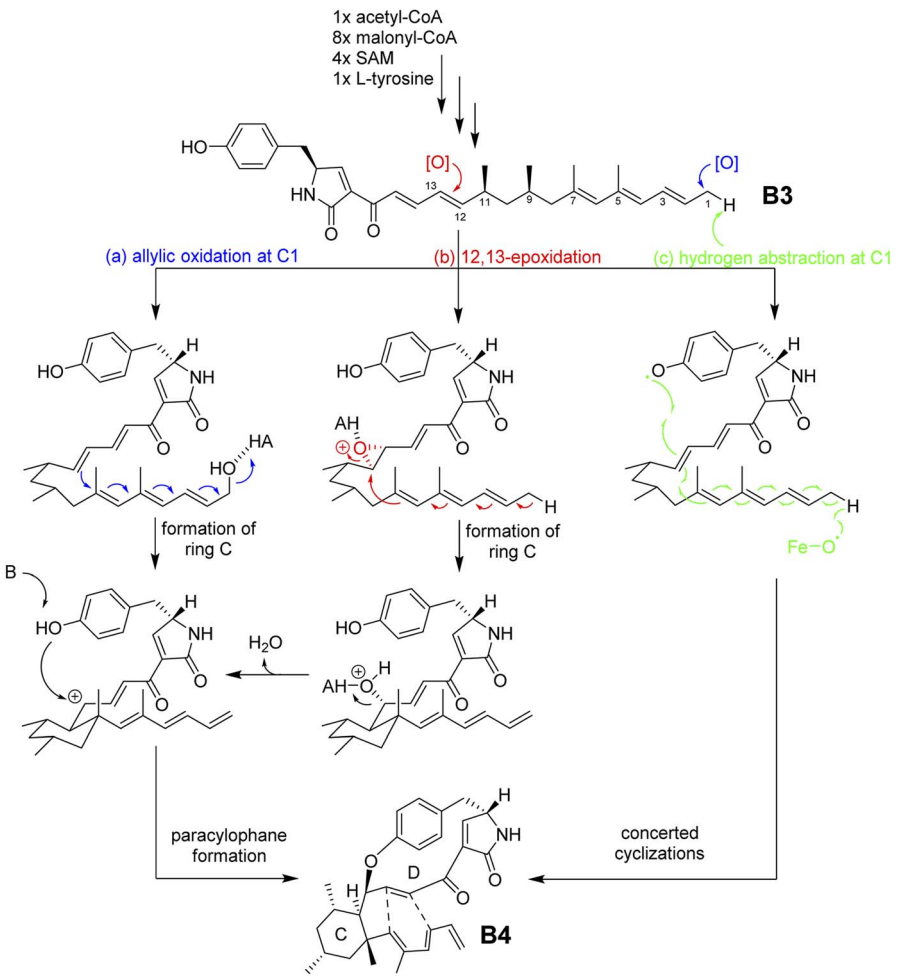

Scheme 3 Proposed mechanisms for the intramolecular cyclization reactions leading to the formation of rings C and D during pyrrocidine biosynthesis, according to Ear *et al.*[28]

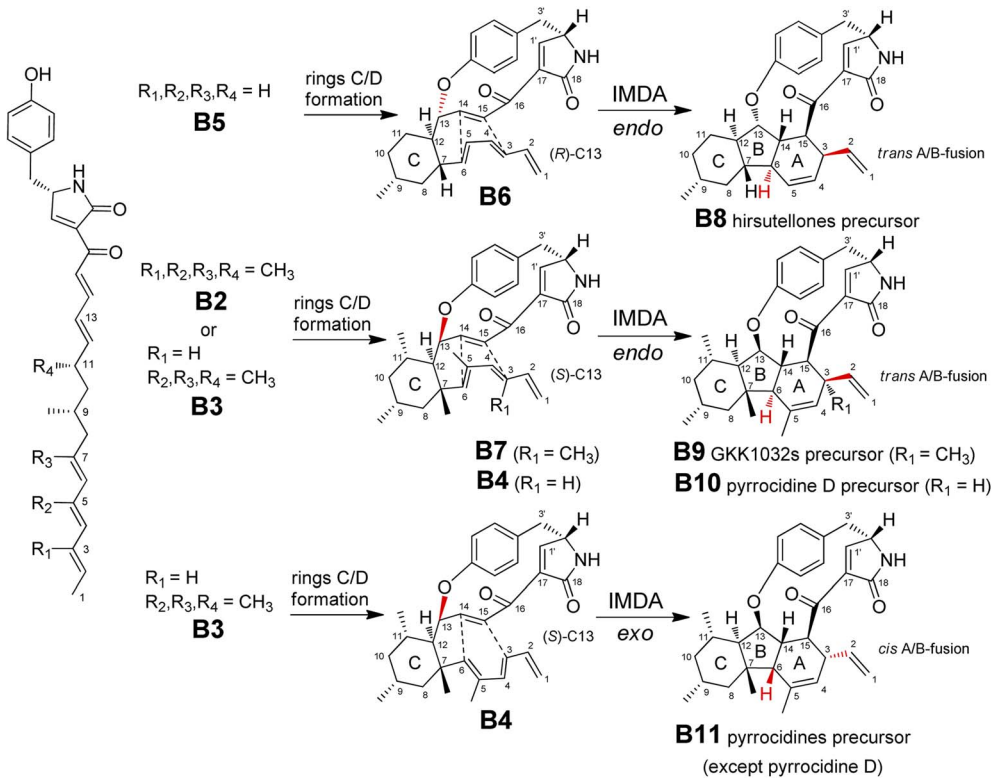

Scheme 4 Proposed biosynthesis of various classes of paracyclophane–decahydrofluorene-containing natural products from the nonaketide linear pyrrolidones **B2**, **B3**, and **B5**. After the initial cyclization to afford rings C and D, the IMDA reaction rationalizes the observed stereochemistry of the A/B ring fusion in hirsutellones, GKK1032 s and pyrrocidines.

polyketide chain configured in an inverse *S*-shaped conformation in the proposed intermediate **B16**, positioning the tyrosine phenol near C13. The fully saturated segment of the chain adopts a chair-like conformation stabilized by equatorial methyl groups at C9 and C11. Deprotonation of the tyrosine phenol to phenolate enables nucleophilic attack at C13 olefin, affording ring D and triggering the conjugated addition of C12 into the triene system at C7, leading to the closure of ring C. A hydride acceptor, presumably the $NAD(P)^+$ co-factor of MDR, may position near C1 to complete the reaction.[22,29] The formation of the *endo*-product **B15**, and not the anticipated *exo*-product **13**, suggested that PydB is not the long-sought Diels–Alderase directing the *exo* IMDA reaction. Further analysis of the BGCs afforded PydY (HP) on a different contig in the *A. zeae* genome. The co-expression of PydY, together with all the aforementioned proteins, led to the formation of **13**. PydY homologues were absent from *P. citrinum* BGC, which, upon heterologous expression and augmentation with PydE, produced the expected $GKK1032A_2$ (**12**) bearing a *trans*-fused A/B ring system. PydY was therefore concluded to be the Diels–Alderase (pericyclase) responsible for the formation of *cis*-fused A/B ring system in pyrrocidine biosynthesis.[22]

Chen *et al.* cultivated *S. zeae* on different media under varying cultivation periods and identified paracyclophane–decahydrofluorene compounds, including pyrrocidine D keto-form **B15**, enol-form **B15a**, and trichobamide B (**B17**), besides the previously isolated major metabolites **13** and **34**.[30] Genome sequencing, followed by the systematic inactivation of PKS-NRPS genes in each predicted BGC, pinpointed that the *prc* cluster is responsible for pyrrocidine biosynthesis (Table 1). Single-gene knockouts of *prc* were generated and cultivated, and their metabolites were analysed by LC-HRMS and characterized by NMR spectroscopy. Initially, the deletion of *prcI* resulted in the disappearance of **13** and **B15**/**15a**, but not **34**, indicating that PrcI is responsible for the reduction of the olefinic bond in the pyrrolidone ring. Subsequently, the deletion of *prcX* resulted in a pronounced reduction in the accumulation of *exo*-products (**13** and **34**), accompanied by the formation of *endo*-products previously undetected in the wild-type fungus, such as pyrrocidine E (**B18**), inferring the contribution of PrcX in directing the IMDA reaction towards the formation of *exo*-type pyrrocidines. The deletion of *prcH* did not result in the impairment of pyrrocidine production but led to the accumulation of an all-*E* polyene alcohol shunt product related to **B3**. PrcH was suggested to prevent the reduction of the putative aldehyde intermediate **B19** released from PKS-NRPS to give shunt products or to promote the catalysis of the otherwise spontaneous Knoevenagel condensation affording **B3**.

Analysis of the metabolites produced after the individual deletion of *prcB*, *D* and *E* genes afforded multiple compounds with complex polycyclic and macrocyclic structures. Mutants lacking *prcB* could not produce pyrrocidines and accumulated shunt products that did not contain the characteristic trimethyl cyclohexane ring, indicating that PrcB is responsible for the

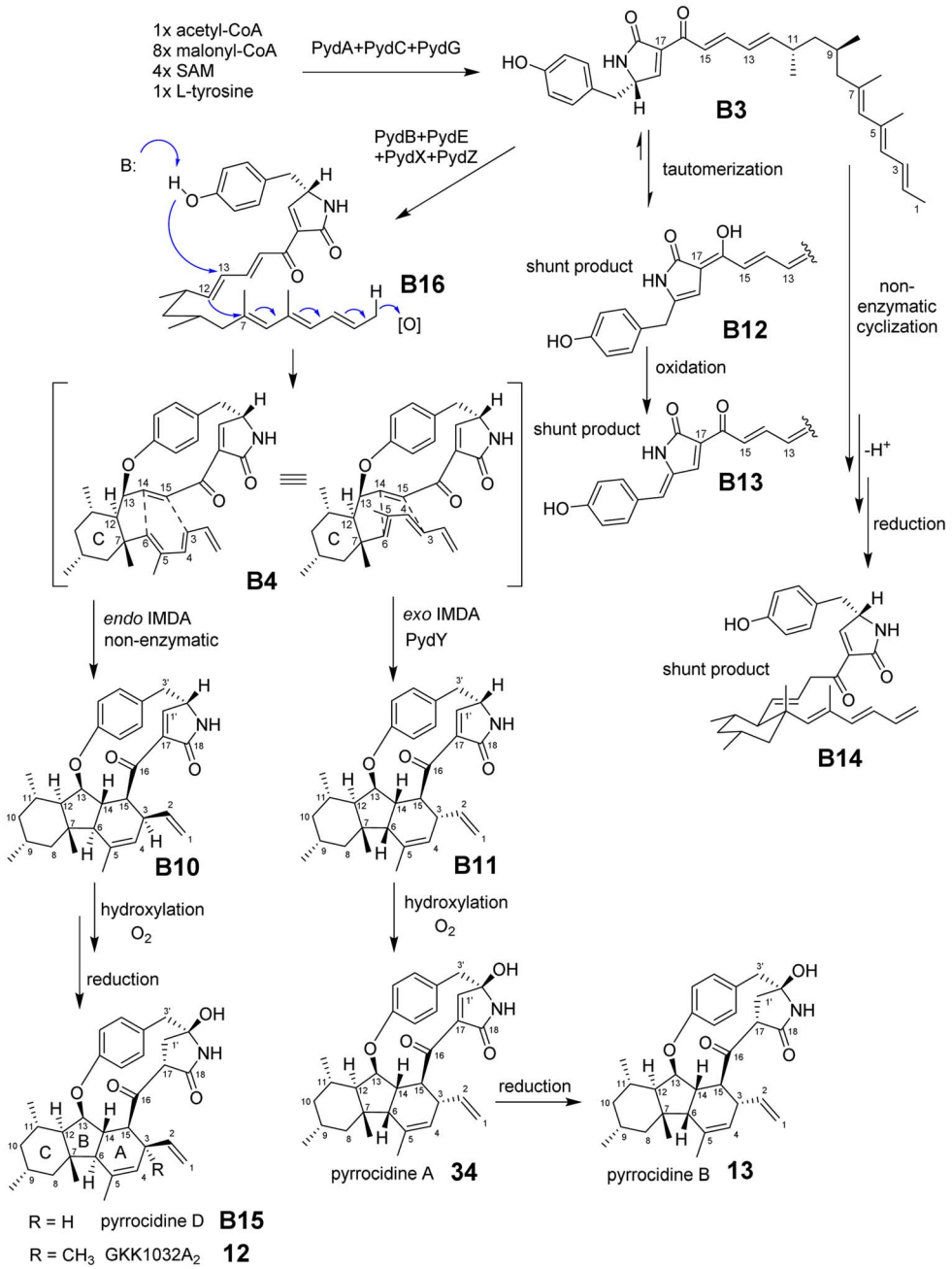

Scheme 5 Proposed biosynthetic pathway for the production of **13** in *S. zeae*, as elucidated by Ohashi *et al.*[22]

initial cyclisation of **B3**, affording ring C in **B20**. In contrast, Δ*prcD* mutants accumulated intermediates bearing ring C but lacking downstream oxidization, allowing the functional assignment of PrcD as the enzyme responsible for the hydroxylation of the pyrrolidone ring of **B20** to **B21** (Scheme 6). Disruption of *prcE* resulted in shunt products containing ring C, but not pyrrocidines, indicating that PrcE is essential for the formation of the strained paracyclophane ring D. Trials to reconstitute the predicted activities of PrcB, D, or E using functional expression of *E. coli* were unsuccessful, presumably due to the insolubility of the membrane-associated PrcB and the pronounced cytotoxicity of PrcD and E. No detectable conversion was observed upon feeding predicted intermediates as substrates in Δ*prcB* or Δ*prcE* mutants.

According to Chen *et al.*,[30] the biosynthesis would proceed as shown in Scheme 6. In brief, the PKS-NRPS (PrcA), together with its partner enoyl reductase (PrcC), constructs the linear aldehyde **B19**, which subsequently undergoes a Knoevenagel condensation, likely catalysed or assisted by PrcH, to yield the pyrrolidone **B3**. Ring C is installed by PrcB, accompanied by the rearrangement of the double bonds to give intermediate **B20**. The pyrrolidone moiety is then hydroxylated by PrcD to afford **B21**, although initial hydroxylation, followed by cyclization, is also comprehensible. PrcE catalyses the formation of the

Table 1 Comparative functional annotation of enzymes encoded by the pyrrocidine biosynthetic gene cluster (BGC) in *S. zeae*. Prc and Pyd denote the same gene cluster, with alternative gene names and functions as assigned by Chen *et al.*[30] and Ohashi *et al.*,[22] respectively

Prc	Bioinformatic assignment	Biochemical function by Chen *et al.*[30]	Pyd	Bioinformatic assignment	Biochemical function by Ohashi *et al.*[22]
A	PKS-NRPS	Formation of the linear aldehyde	A	PKS-NRPS	Formation of the linear
C	*trans*-Acting enoyl reductase	nonaketide	C	*trans*-Acting enoyl reductase	3-pyrrolin-2-one nonaketide
H	α/β-Hydrolase	Condensation to afford the pyrrolidone ring	G	α/β-Hydrolase	
B	Lipocalin-like protein	Formation of ring C	B	Putative Diels–Alderase and hexane cyclase	Formation of ring C and paracyclophane ring D
I	*trans*-Acting enoyl reductase	Reduction of the olefinic bond in the pyrrolidone ring	E	Medium-chain dehydrogenase/reductase	
D	Integral membrane protein	Hydroxylation of the pyrrolidone ring	X	Small hypothetical protein	
E	Integral membrane protein	Formation of paracyclophane ring D	Z	Small hypothetical protein	
X	Lipocalin-like protein	Promoting the *exo*-IMDA reaction	Y	Small hypothetical protein	Promoting the *exo*-IMDA reaction

paracyclophane ring D. Finally, PrcX enables an enantioselective *exo* IMDA reaction to form a *cis*-fused A/B ring junction, yielding pyrrocidine A (**34**), which is subsequently reduced by PrcI to give **13**.

Computational analyses, including homology modelling of PrcB and molecular docking with **B3**, were performed to understand the mechanism of ring C formation. Docking studies suggested that part of the hydrocarbon chain of intermediate **B3** (C7–C12) attains a chair-like conformation within the active site of PrcB, with an axial methyl group at C7 and equatorial C9 and C11, matching the stereochemical arrangement observed in ring C. PrcB was proposed to initiate the reaction by deprotonation at C1 by R265, triggering double-bond isomerization along the polyene chain and promoting the intramolecular attack of C7 onto C12 to generate ring C, followed by protonation at C15 by E115. Stabilization of the resulting *trans*-configured C13–C14 olefin would in turn favour subsequent cyclophane formation catalysed by PrcE. PrcE was proposed to operate through a redox-active disulfide bond, acting as an electron acceptor during oxidative paracyclophane formation. This step was suggested to involve the transient formation of a cysteine-quinone adduct between the C4′ of intermediate **B21** and an active-site cysteine. Introduction of the sp^3 character at C4′ and a temporary loss of aromaticity would relieve conformational constraints, allowing C13 to approach the quinone oxygen. The subsequent intramolecular attack of C13 on the quinone oxygen would close the cyclophane ring, accompanied by the release of the cysteine residue and re-aromatization, ultimately yielding the characteristic trapped, distorted benzene ring (Scheme 7). Notably, this mechanism accounts for the (*S*)-C13 stereochemistry observed in pyrrocidines and GKK1032 s, whereas the mechanism previously proposed by Ohashi *et al.* would instead result in the (*R*)-C13 configuration. While (*R*)-C13 is indeed found in hirsutellones, the corresponding biosynthetic gene cluster has not yet been identified.[22]

The studies by Ohashi *et al.*[22] and Chen *et al.*[30] were focused on the same fungus but employed different strategies, namely, heterologous expression *versus* stepwise single-gene deletions. Both studies confirmed the role of PKS-NRPS in assembling the linear pyrrolinone nonaketide precursor previously proposed by Oikawa.[27] Additionally, both asserted the need for multiple auxiliary proteins for the construction of the strained paracyclophane and the decahydrofluorene rings. The studies independently discovered that PydY/PrcX is the long-sought pericyclase promoting *exo*-selective IMDA cyclization to generate the *cis*-fused A/B ring system. However, they diverge in the interpretations of the upstream cyclization steps: Ohashi *et al.*[22] proposed a cooperative multiprotein complex to mediate oxidative cyclization, whereas Chen *et al.*[30] clarified the roles of the individual proteins and challenged the cyclization mechanism proposed by Ohashi *et al.*[22] Notably, the two groups adopted different nomenclatures for identical proteins; therefore, an overview of the corresponding gene names and their experimentally assigned functions is provided in Table 1 to facilitate direct comparison.

Another study by Liu *et al.*[31] investigated the biosynthesis of the structurally related xenoacremones in the Chinese mangrove endophyte *Xylaria sinensis* ML-31. Genome sequencing, followed by bioinformatic analysis, identified the *xen* BGC to be responsible for xenoacremone biosynthesis. Through a combined approach involving gene deletion and heterologous expression, accompanied by metabolite identification, the roles of individual proteins in the cluster were clarified. Liu *et al.* proposed that the biosynthesis proceeds through the formation of a tyrosine-nonaketide derivative analogous to **B3** but carrying only two methyl substitutions by the action of XenE (PKS-NRPS) and its associated XenG (*trans*-ER).

The formation of a pyrrolidone condensation product is catalysed by XenA (α/β-hydrolase). The linear pyrrolidone is converted to the xenoacremone scaffold by three hypothetical proteins. XenF (PrcB/PydB homologue) catalyses the formation of ring C, presumably through a [1,11]-sigmatropic rearrangement, XenD (PrcD/PydX homologue) installs an epoxide on the pyrrolidone ring, and XenC (PrcE/PydZ homologue) forms the paracyclophane ring (Scheme 8). The proposed biosynthesis

follows a logic similar to that outlined in the previously discussed studies; however, it assumes that the IMDA reaction proceeds spontaneously and does not identify a homologue to the key pericyclase (PrcX/PydY) responsible for the enantioselectivity.

Taken together, the biosynthetic logic underlying the cyclization steps of the PKS-NRPS-derived linear nonaketide intermediate remains debatable, as evident from the divergent interpretations among the studies by Ohashi *et al.*,[22] Chen *et al.*[30] and Liu *et al.*[31] Ohashi *et al.* achieved the first successful heterologous reconstitution of the pathways. However, their proposed pathway assigns multiple auxiliary proteins (PydB/E/X/Z-PrcB/I/D/E) as a cooperative oxidative-cyclization ensemble without clearly resolving the precise role of each enzyme or the sequence of the cascade they catalyze. Moreover, the proposed phenolate attack/conjugate-addition sequence remains challengeable, as it does not adequately explain either the observed (*S*)-C13 configuration in pyrrocidines and GKK1032A$_2$ or the formation of the highly distorted paracyclophane ring, which bends more than 12° from planarity. In contrast, Chen *et al.*[30] employed native-strain single-gene deletions in *S. zeae* to assign distinct, stepwise functions to the individual enzymes involved (Table 1). For example, Chen *et al.* assigned PydZ/PrcE as the paracyclophane-forming enzyme and provided a computationally supported rationale for aromatic ring distortion. PydZ/PrcE is proposed to transiently dearomatize the substrate through the formation of a cysteine-quinone adduct within its active

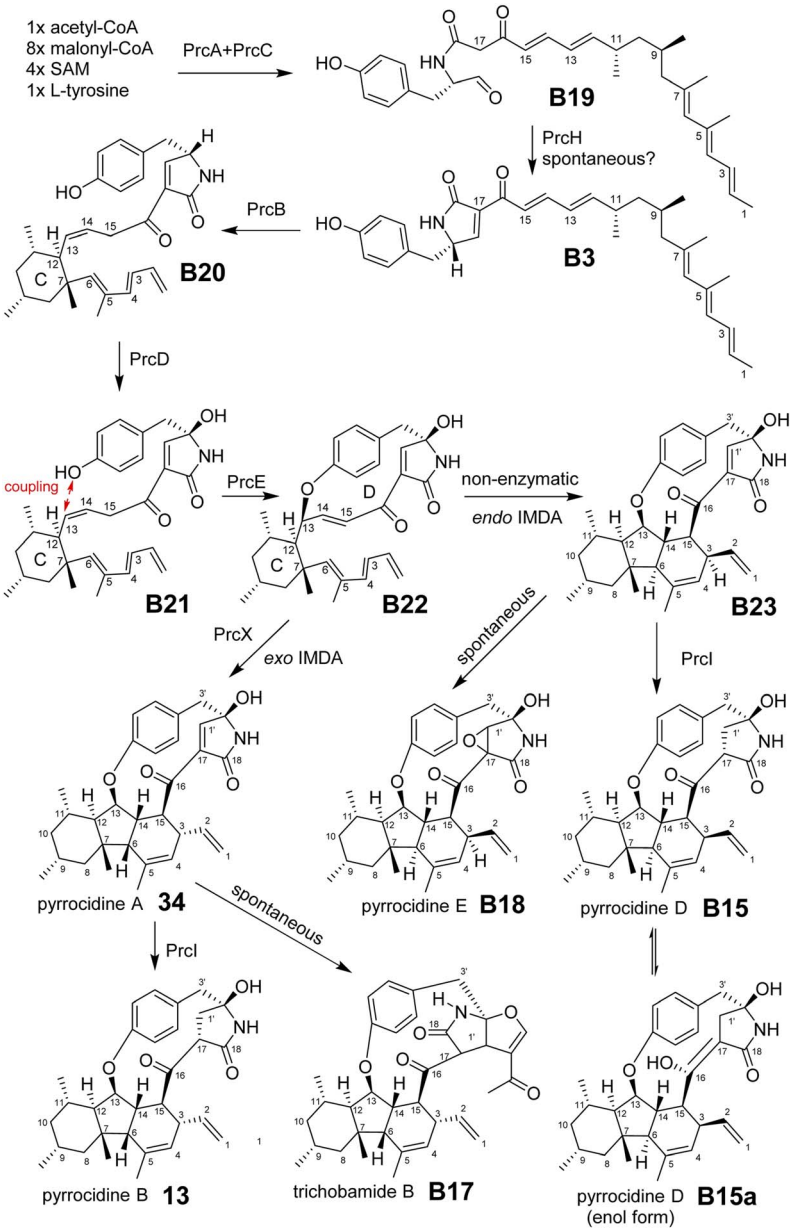

Scheme 6 Proposed biosynthetic pathway for the biosynthesis of pyrrocidines, according to Chen *et al.*[30]

site, thereby lowering the energetic barrier to paracyclophane formation.

Using a combined approach involving targeted gene deletions and heterologous expression, Liu *et al.*[31] elucidated the xenoacremone biosynthetic pathway in *Xylaria sinensis* and proposed that XenF (PydB/PrcB homolog) catalyzes a sigmatropic rearrangement to install ring C. This assumption has been scrutinized by Chen *et al.* and Youwei Chen,[30,32] who employed homology modeling and molecular docking to demonstrate that the linear nonaketide intermediate adopts an "elbow shape" within the active site cavity, positioning the C1 and C15 atoms approximately 10 Å apart. This distance renders a concerted sigmatropic hydrogen migration structurally impossible, as such a process would necessitate a transition state where these two carbons are in proximity. Alternatively, Chen *et al.* proposed a base-catalyzed isomerization-cyclization mechanism facilitated by a conserved tetrad (R265, D87, E85, and E118), highlighting the role of R265 as a general base that deprotonates the terminal methyl at C1 to initiate a double-bond isomerization cascade along the polyene chain.

Although the interpretation proposed by Chen *et al.*[30] offers a chemically more plausible explanation, important limitations remain. Several functional assignments, particularly those involving PydB/PrcB, PydX/PrcD, and PydZ/PrcE, rely mainly on *in silico* analyses rather than direct biochemical evidence. Because heterologous expression in *E. coli* was unsuccessful, potentially due to protein insolubility and cytotoxicity, key mechanistic proposals (such as the arginine-mediated deprotonation by PrcB and the transient dearomatization by PydZ/PrcE) remain speculative and experimentally unverified. Moreover, the metabolites isolated and extensively characterized from mutant strains represent stable shunt products rather than confirmed reactive pathway intermediates. Thus, although Chen's stepwise model is mechanistically attractive and helps rationalize pathway plasticity, it does not definitively disqualify the cooperative oxidative-cyclization ensemble originally proposed by Ohashi *et al.*[22]

The final step leading to the formation of the decahydrofluorene core involves an intramolecular Diels–Alder (IMDA) reaction, a step that distinguishes the *cis*-fused pyrrocidines (arising from an *exo* transition state) from the *trans*-

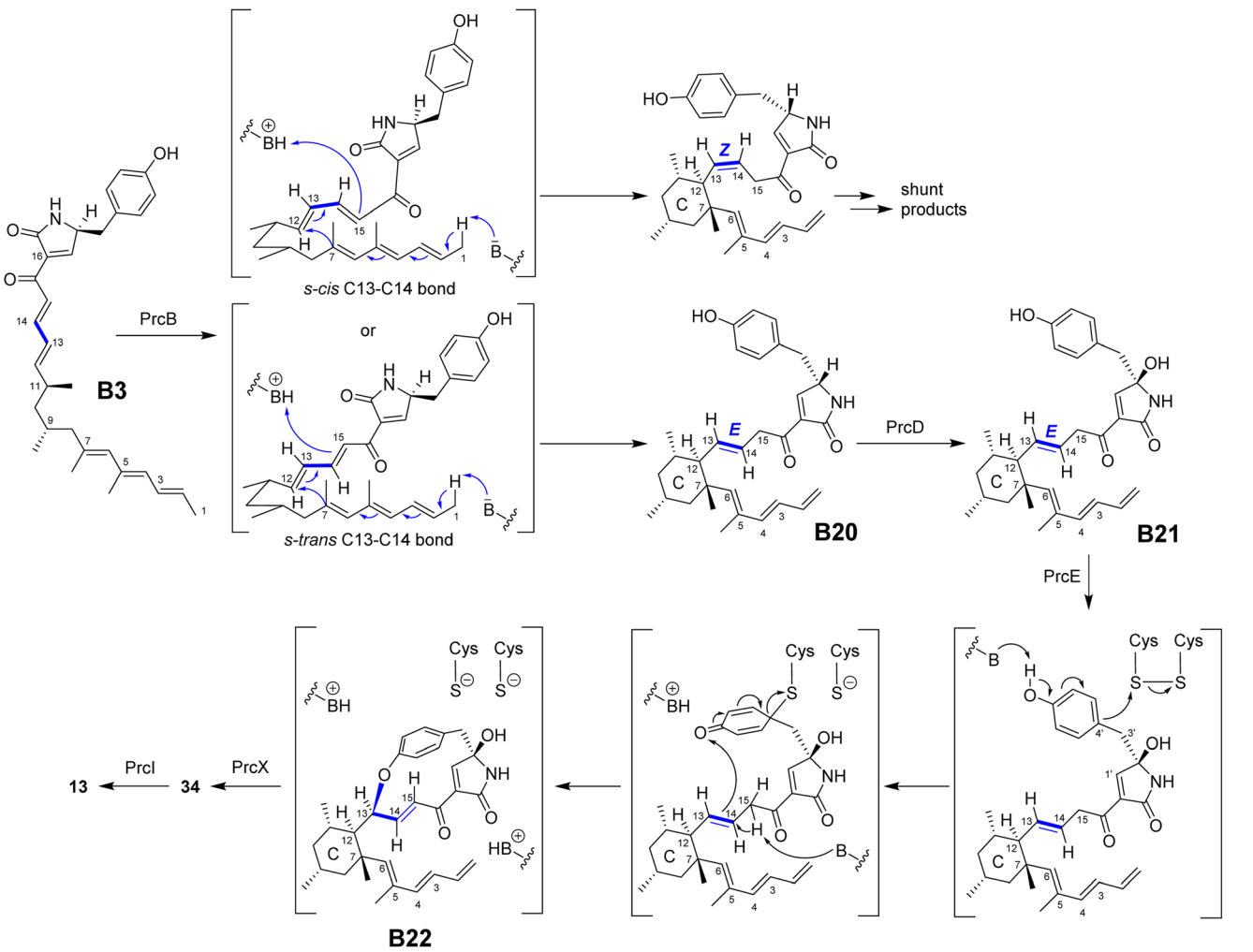

Scheme 7 Mechanism for the formation of the paracyclophane–decahydrofluorene, as proposed by Chen *et al.*[30]

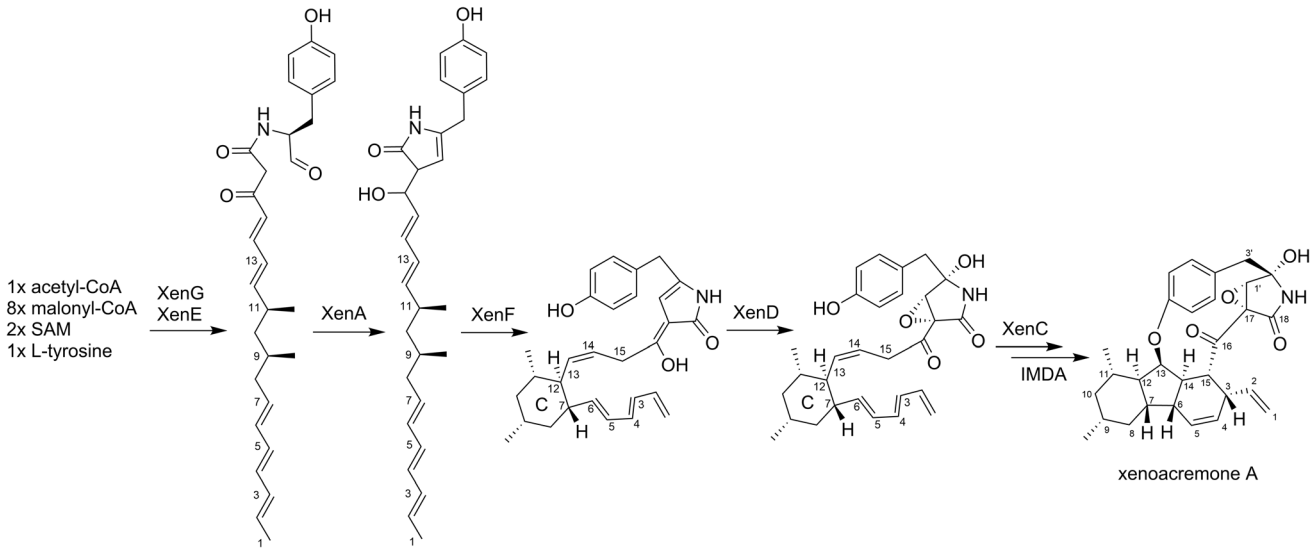

Scheme 8 Biosynthesis of xenoacremone A, as elucidated by Liu *et al.*[31]

fused GKK1032 s and hirsutellones (arising from an *endo* transition state) (Scheme 4). While the *endo*-mode is chemically favored, the exclusive formation of *exo*-selective adducts in pyrrocidine-producing organisms indicates a requirement for enzymatic control. Ohashi *et al.*[22] initially characterized PydY/PrcX as an essential pericyclase mandatory for this chemically unfavorable *exo*-cyclization step. However, Chen *et al.*[30] demonstrated that *cis*-fused pyrrocidines were still produced in small amounts in Δ*prcX* mutants. This observation led Chen to propose that PydY/PrcX functions as a conformational template that controls the transition-state manifold through active-site shape complementarity rather than acting as a mandatory covalent catalyst. Although Liu *et al.*[31] proposed a nonenzymatic spontaneous IMDA step in xenoacremone biosynthesis, this assignment may be incomplete. Chen's reanalysis of the *xen* locus identified a truncated *pydY*/*prcX*-like homolog (*xenX*) at the BGC boundary.[32] Given the stereo-directing role of PrcX/PydY in the related pyrrocidine biosynthesis, and because Liu's XenX-deficient heterologous reconstitution produced xenoacremones only as minor products alongside additional isomeric peaks, XenX may constitute a missing factor for the terminal IMDA reaction in xenoacremone biosynthesis.

Indeed, Diels–Alderases represent a diverse functional designation for enzymes that accelerate or stereochemically control [4 + 2] cycloaddition reactions in various natural product biosynthetic pathways.[33,34] Diels–Alderases do not constitute a single homogeneous enzyme family with a common protein fold. Instead, they appear to have evolved independently from multiple unrelated enzyme classes, including oxidoreductases,[35] methyltransferases,[36,37] and lipocalin-like synthases.[38,39] They range from stand-alone pericyclases, which accelerate the reaction rate, to enzymes or domains that function mainly as "entropy traps", preorganizing the substrate in favor of a specific regio- and stereo-chemical outcome. Prominent examples of such entropy traps are the lipocalin-like decalin synthases. For example, CghA, involved in the biosynthesis of the decalin–tetramic acid derivative Sch 210972, is responsible for promoting the *endo*-IMDA reaction to the linear precursor, as evident by the formation of a mixture of *endo* and *exo* products in the Δ*CghA* mutants.[40] Similarly, Fsa2 is responsible for *endo*-selective decalin formation in the equisetin biosynthetic pathway. Genetic studies have demonstrated that in Δ*Fsa*2 mutants, the unstable intermediate undergoes spontaneous cyclization, resulting in a loss of stereochemical fidelity and the production of both *endo*- and *exo*-selective adducts.[38] The PydY/PrcX lipocalin-like proteins in pyrrocidine biosynthesis are suggested to function in a similar manner. The formation of minor amounts of *exo*-products in Δ*prcX* mutants suggests that PydY/PrcX acts as a conformational template that biases the transition-state manifold rather than being an absolute requirement for the reaction. However, further research is needed to definitively classify PydY/PrcX as either a bona fide pericyclase or a passive conformational mold. Future studies should include *in vitro* enzyme assays to quantify catalytic rate enhancement and stereochemical control, as well as high-resolution substrate- or intermediate-bound crystal structures, to reveal how the enzyme shapes the IMDA transition state.

3. Chemistry and biology of pyrrocidines and hirsutellones

To date, fifty-five pyrrocidine and hirsutellone derivatives have been isolated from various fungal genera. Herein, these metabolites are categorized and discussed according to the taxonomic classification of their producing fungal sources; additionally, their reported biological activities are detailed where applicable. Note: for organizational clarity, the biosynthetic pathways and precursors discussed in Section 2 are designated using alphabetic identifiers (**A**, **B**, and **C**), whereas isolated compounds and their derivatives discussed in Section 3

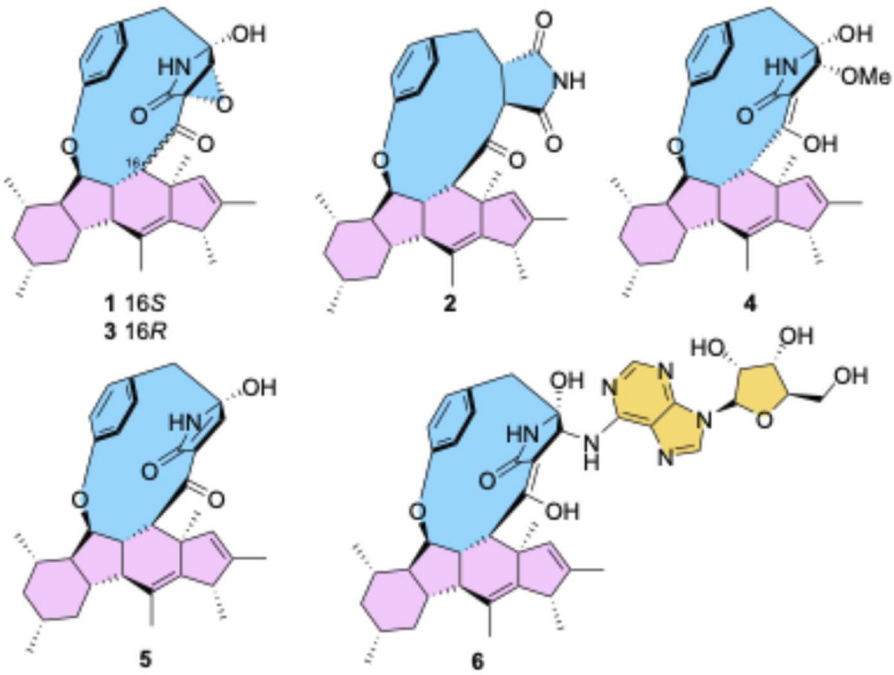

Fig. 1 Chemical structures of 1–6. Pink shading represents the polyketide-derived skeleton (the decalin/PKS component). Blue shading distinguishes the amino acid-derived macrocyclic framework (the NRPS/tyrosine-derived component).

are numbered sequentially using Arabic numerals starting with **1**.

3.1. Fungi of the class Dothideomycetes

3.1.1. Fungi of the subclass Pleosporomycetidae

3.1.1.1. Fungi of the order Pleosporales

3.1.1.1.1. Fungi of the family Didymellaceae. 3.1.1.1.1.1.Genus Didymella (*MycoBank ID 1548*) Chemical investigation of the marine endophytic fungus *Didymella* sp., isolated from *Pluchea indica*, collected in China from the Province of Guangxi, led to the isolation of two previously undescribed polyketide alkaloid derivatives, namely, phomapyrrolidone C (**1**) and phomapyrrolidone A (**2**), along with three previously unreported analogues, namely, ascomylactams A (**3**), B (**4**), and C (**5**) (Fig. 1). Compounds **1–5**, along with EPI as a positive control, were examined for their cytotoxic effect against MDA-MB-435, SNB19, HCT116, NCI-H460, and PC-3 cancer cell lines using the MTT method, where all isolated compounds displayed weak to mild effects with IC_{50} values ranging from 4.9 to >50 μM, compared to the positive control (IC_{50} values ranging from 0.12 to 5.7 μM).[41] Ariantari *et al.* reported the isolation of didymellanosine (**6**)—the previously undescribed alkaloid derivative represented the first example of a pyrrocidine derivative conjugated with adenosine (Fig. 1)—along with the previously mentioned analogues **2** and **5**, from the organic extract of the endophytic fungus *Didymella* sp., obtained from *Terminalia catappa* leaves collected in Indonesia from the south of Bali. Among the isolated compounds, compound **6** displayed a strong cytotoxic effect towards the L5178Y tumour cell line compared to kahalalide F as a positive control, with IC_{50} values of 2.0 and 4.3 μM, respectively. Furthermore, **6** was active against Ramos and Jurkat J16 human cancer cell lines, with IC_{50} values of 3.3 and 4.4 μM, respectively, as well as against MRC5 cells, with an IC_{50} value of 21.2 μM, indicating its mild selectivity against cancer cells. Moreover, it displayed a moderate NF-κB inhibitory activity, with an IC_{50} value of 45.4 μM. Additionally, compounds **2**, **5** and **6**, were tested for their antibacterial effect against a panel of Gram-positive and -negative bacterial strains, including *M. tuberculosis*, *S. aureus*, *E. faecalis*, *E. faecium* and *A. baumannii*, using rifampicin and moxifloxacin as positive controls; while all remaining compounds were inactive against *M. tuberculosis*, compound **2** exhibited weak inhibitory activity against *S. aureus*, *E. faecalis*, and *E. faecium*. In contrast, compounds **5** and **6** exhibited significantly more potent antibacterial activity against these strains, with MIC values of 12.5–100 μM, 3.1–6.3 μM, and 3.1–12.5 μM, respectively. Similarly, they exhibited an inhibitory effect against the Gram-negative bacterium *A. baumannii*, displaying MIC values of 12.5, 3.1, and 3.1 μM, respectively.[42]

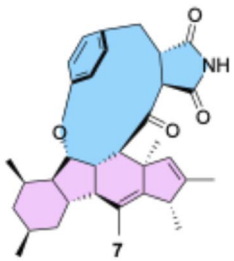

Fig. 2 Chemical structure of 7.

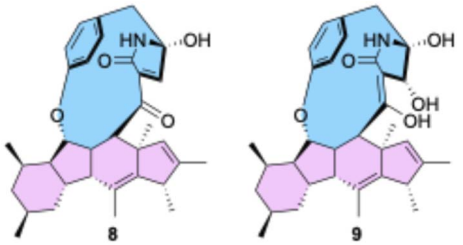

Fig. 3 Chemical structures of **8** and **9**.

Fig. 5 Chemical structure of **11**.

3.1.1.1.1.2.Genus Phoma (*MycoBank ID 9358*) The previously undescribed polyketide alkaloid analogue phomapyrrolidone B (**7**) (Fig. 2), together with the previously mentioned analogues **1** and **2**, was isolated from the endophytic seed-derived fungus *Phoma* sp. The isolated compounds were evaluated for their antitubercular activity using rifampin and isonicotinylhydrazine as positive controls, where they displayed weak effects, with MIC values of 5.2 and 13.4 μM, 20.1 and 41.1 μM, 0.07 and 0.1 μM, 5.2 and 13.4 μM, and 0.03 and >17.5 μM, when assessed using the MABA and LORA assays, respectively. Additionally, their cytotoxicity was evaluated against the Vero cell line, where all compounds displayed potent cytotoxic activity compared to rifampin as the positive control, showing IC_{50} values of 19.4, 17.7, 17.1, and 109.0 μM, respectively. Furthermore, all isolated compounds lacked antiproliferative activity when evaluated against a panel of human cancer cell lines at the highest tested concentration.[43]

3.1.1.1.2. Fungi of the family Pleosporaceae. 3.1.1.1.2.1.Genus Embellisia (*MycoBank ID 127066*) Embellicines A (**8**) and B (**9**) (Fig. 3), two previously undescribed polyketide alkaloid derivatives, were obtained from the plant-derived fungus *Embellisia eureka*, isolated from *Cladanthus arabicus* stems, collected in Morocco. Both compounds were tested for their cytotoxic effect against K562 and A549, and both of them displayed potent cytotoxic effects, with IC_{50} values of 3.473, 2.855, 1.282, and 1.202 μM and 0.92, 0.32, 0.25, and 0.21 μM after 8, 24, 48, and 72 h, respectively, against K562 cells. Furthermore, **9** displayed a moderate cytotoxic effect against PBMC cells, with an IC_{50} value of 12.8 μM. Moreover, both compounds inhibited TNFα-induced NF-κB transcriptional activity, with IC_{50} values of 3 and 0.35 μM, respectively. Additionally, the antiproliferative effect of compound **9** was evaluated against K562 and A549 cancer cells, demonstrating significant activity at concentrations higher than or equal to 0.5 μM.[44]

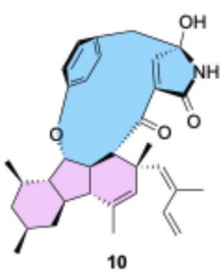

Fig. 4 Chemical structure of **10**.

3.1.1.1.2.2.Genus Lewia (*MycoBank ID 104458*) Pyrrocidine C (**10**) (Fig. 4), a previously undescribed polyketide alkaloid derivative, was isolated from the ethyl extract of the plant-derived fungus *L. infectoria*. Compound **10** was evaluated for antimicrobial activity against *Candida albicans* and *Staphylococcus aureus*, utilizing fluconazole and oxacillin as positive controls. It exhibited weak activity against *C. albicans* (MIC > 128 *vs.* 4 μM for fluconazole) and moderate potency against *S. aureus* (MIC = 2 *vs.* 4 μM for oxacillin). Furthermore, compound **10** was evaluated for its cytotoxicity against KB, MRC5, and MDA-MB-435 cell lines using docetaxel and doxorubicin as positive controls; it was found to be inactive (IC_{50} values of >10 μM), whereas the reference drugs displayed highly potent activity (IC_{50} values of 0.0002, 0.02, and 0.0005, respectively).[45]

3.1.1.1.3. Fungi of the unidentified family. 3.1.1.1.3.1.Genus Trichobotrys (*MycoBank ID 10275*) Trichobamide A (**11**) (Fig. 5), a previously undescribed pyrrocidine analogue possessing an unprecedented tetrahydro-5*H*-furo[2,3-*b*]pyrrol-5-one residue, was isolated from the marine-derived fungus *Trichobotrys effusa*. It displayed significant antiproliferative activity against SNB19 and U251 glioma cell lines in a concentration- and time-dependent manner, which downregulated antiapoptotic genes and upregulated downstream proapoptotic pathways *via* the activation of P53 expression.[46]

3.2. Fungi of the class Eurotiomycetes

3.2.1. Fungi of the subclass Eurotiomycetidae

3.2.1.1. Fungi of the order Eurotiales

3.2.1.1.1. Fungi of the family Aspergillaceae. 3.2.1.1.1.1.Genus Penicillium (*MycoBank ID 9257*) Becker *et al.* reported the isolation of GKK1032A2 (**12**), a previously undescribed analogue of pyrrocidine B (**13**) (Fig. 6), from the culture of *Penicillium* sp. Even though compound **12** was found to be inactive against Colo-320 cell lines, it displayed cytotoxic activity against the Jurkat cell line, with an IC_{50} value of 10 μM. Additionally, compound **13** displayed antitumour effects against the HeLa S3 tumour cell line, with an IC_{50} value of 25 μM. Furthermore, compounds **12** and **13** inhibited the conidial germination of *M. oryzae*, with IC_{50} values of 3 and 2.5 μM, respectively. Moreover, when both compounds were evaluated for phytotoxicity against *L. sativum*, *O. sativa*, *S. italica*, and *T. aestivum*, only compound **12** exhibited weak activity against *L. sativum*, *S. italica*, and *T.*

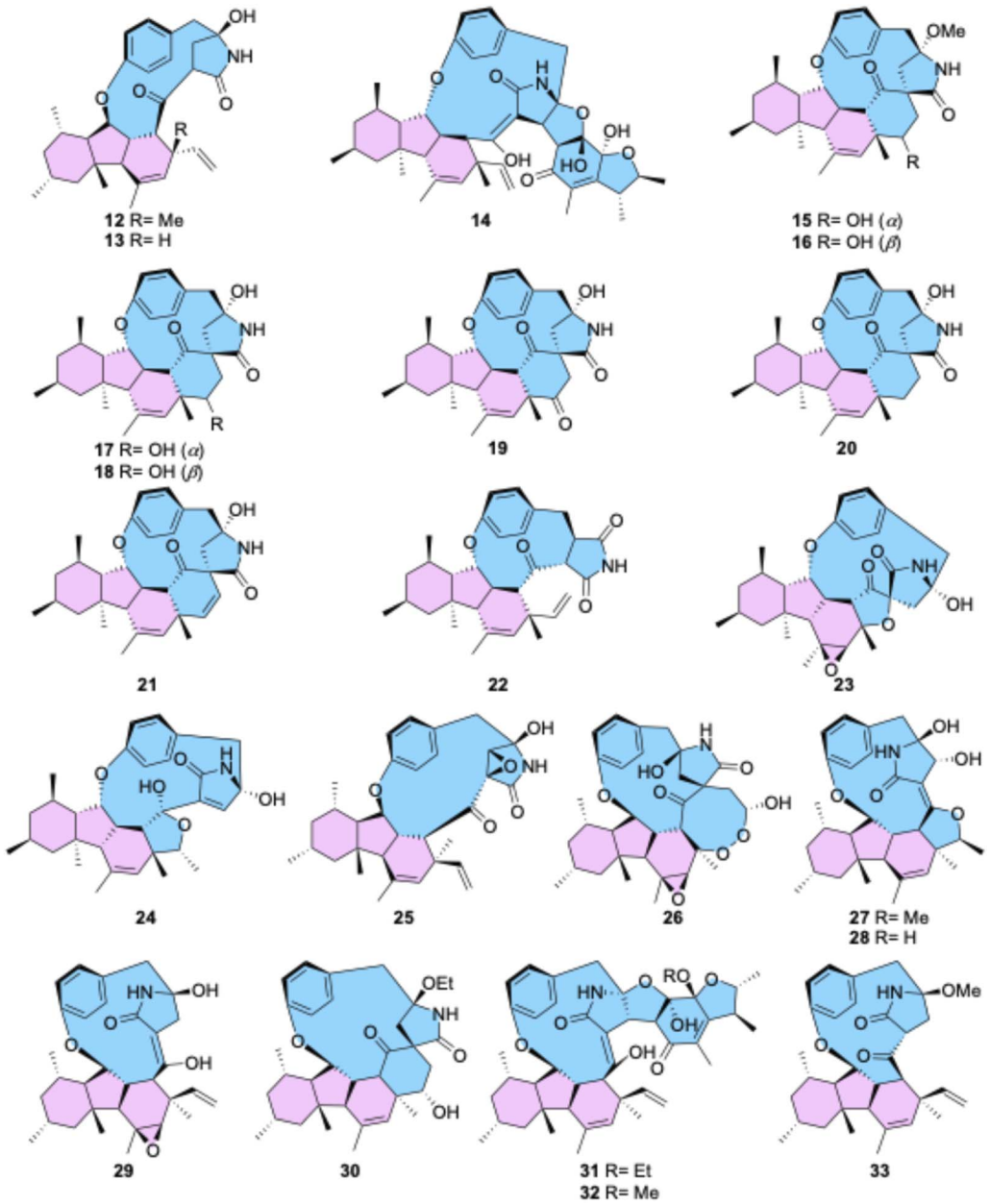

Fig. 6 Chemical structures of 12–33.

aestivum, with IC_{50} values ranging from 50–>100 μM. Additionally, antimicrobial screening against a panel comprising *B. brevis*, *B. subtilis*, *M. luteus*, *E. dissolvens*, *S. aureus*, *C. albicans*, *M. oryzae*, *M. miehei*, *N. coryli*, and *P. variotii* revealed that only compound **13** was active, showing selective potency against *S. aureus* and *M. oryzae*, with MIC values of >10 μM.[47]

Chemical investigation of the marine-derived fungus *Penicillium* sp., isolated from the wild crab *P. crassipes*, led to the isolation of a previously undescribed analogue, namely, penicipyrrodiether A (**14**) (Fig. 6). Compound **14** was evaluated for antibacterial activity against *S. aureus* (MRSA) and *E. coli*, exhibiting mild to weak activity with MIC values of 5.0 and 34.0 μM, respectively, compared to the positive control, gentamicin (MIC values of 0.7 and 0.9 μM, respectively). Additionally, it exhibited moderate antiproliferative activity against a panel of glioma cell lines (rat C6 and human U251, U87-MG, and SHG-44), with IC_{50} values ranging from 11.32 to 29.10 μM. In comparison, the positive control, doxorubicin, displayed significantly higher potency, with IC_{50} values ranging between 0.7 and 9.61 μM.[48] Further examination of the same fungal strain by the same research group led to the isolation of more previously undescribed pyrrospirone derivatives, namely, pyrrospirones C (**15**), D (**16**), E (**17**), F (**18**), G (**19**), H (**20**), and I (**21**), along with the previously described analogue GKK1032B (**22**) (Fig. 6).

Compounds **15–21** were evaluated for their antiproliferative effects against U251, SHG44, U87MG, and C6 tumour cells, utilizing doxorubicin (DOX) as a positive control. All isolated

compounds displayed moderate to potent activity, with IC_{50} ranged between 1.06 and 26.64 μM (*cf.* IC_{50} = 0.47–8.03 μM for DOX). In the antibacterial screening against *E. coli* and MRSA, compound **5** was inactive (MIC > 50 μM), whereas the remaining analogues exhibited mild to strong inhibition, with MIC values ranging between 2.0 and 19.0 μM (gentamicin control, MIC = 1.0 and 0.5 μM, respectively). Additionally, all isolated compounds lacked antifungal activity compared to the positive control, amphotericin B.[49]

Further chemical investigation of the same fungal strain cultured in a potato dextrose broth (PDB) medium yielded pyrrospirone J (**23**) (Fig. 6), which had been detected in a previous work without structural elucidation, together with a novel analogue, penicipyrroether A (**24**) (Fig. 6). Both compounds were evaluated for cytotoxic activity against U87MG and U251 tumour cells. Compound **23** exhibited IC_{50} values of 10.52 and 17.92 μM, respectively, while **24** showed higher potency, with IC_{50} values of 1.64 and 5.50 μM, respectively (*cf.* IC_{50} = 1.20 and 8.03 μM for doxorubicin, respectively). Furthermore, when tested against *E. coli* and MRSA, only compound **24** was active, demonstrating MIC values of 3.0 and 1.7 μM, respectively, compared to the reference antibiotics gentamicin (MIC = 1.44 and 0.36 μM) and vancomycin (MIC = 0.20 μM against MRSA).[50]

Chemical examination of the mangrove-derived fungus *Penicillium* sp. led to the isolation of a previously undescribed polyketide alkaloid derivative, GKK1032C (**25**) (Fig. 6), together with the known analogues **12**, **17**, **18**, and **22**. These compounds were evaluated for their antibacterial activity against Gram-positive strains [methicillin-resistant and methicillin-susceptible *S. aureus* (MRSA and MSSA, respectively)] and Gram-negative pathogens (*E. coli*, *P. aeruginosa*, and *A. baumannii*). All tested metabolites displayed weak to potent inhibitory activity, with MIC values ranging from 1.6 to >25.8 μM, compared to the positive controls vancomycin (MIC = 1.0 to >32.0 μM) and meropenem (MIC = 0.00625 to >32.0 μM).[51]

The previously mentioned analogue **22** was recovered from the endophytic fungus *Penicillium citrinum*, which was isolated from the leaf tissue of the medicinal plant *D. officinale*. When evaluated for antiproliferative activity against U2OS and MG63 osteosarcoma cell lines at a concentration of 20 μM, compound **22** exhibited strong growth inhibition, with inhibition rates of 98.59% and 97.67%, respectively. In comparison, the positive control, doxorubicin, showed inhibition values of 68.32% and 88.19% at a concentration of 0.5 μM, respectively. Additionally, compound **22** demonstrated cytotoxic effects against MDA-MB-231, A549, HeLa, MG63, and U2OS lines, yielding IC_{50} values of 10.72, 14.60, 19.83, 3.49, and 5.07 μM, respectively, whereas doxorubicin displayed IC_{50} values of 0.36, 0.45, 0.43, 0.27, and 0.44 μM, respectively.[52]

Seven previously undescribed hirsutellone derivatives, namely, perpyrrospirone A (**26**) and penicilliones B–G (**27–32**), along with the previously reported analogue GKK1032A1 (**33**) (Fig. 6) and the known analogues **12**, **14**, **15**, **16**, **19**, **22**, **24**, and **25**, were isolated from the marine crab-derived fungus *Penicillium citrinum*. The fungus was recovered from a sample of *Chiromantes haematocheir* collected in Zhejiang, China. Compounds **12**, **14**, **15**, **16**, **19**, **22**, **24**, **25**, **26**, **31**, and **33** were evaluated for cytotoxic activity against HepG2, MGC803, MCF-7, Bel-7402, MDA-MB-231, and HeLa cell lines. Among them, compounds **12**, **19**, **25**, **26**, and **32** exhibited significant antitumor effects against the tested lines, with IC_{50} values ranging between 0.76 and 38.9 μM. In comparison, the positive controls, 5-fluorouracil (IC_{50} = 2.8 to >50 μM) and doxorubicin (IC_{50} = 0.21–6.6 μM), displayed typical reference potencies.[53]

3.3. Fungi of the class Sordariomycetes

3.3.1. Fungi of the subclass Hypocreomycetidae

3.3.1.1. Fungi of the order Hypocreales

3.3.1.1.1. Fungi of the family Bionectriaceae. 3.3.1.1.1.1.Genus Acremonium (*MycoBank ID 519595*) Chemical investigation of the maize-derived fungus *Acremonium zeae* led to the isolation of the previously mentioned polyketide alkaloid derivative **13**, along with the known analogue pyrrocidine A (**34**) (Fig. 7). Both compounds were evaluated for antifungal activity against *F. verticillioides* and *A. flavus* using the paper disc method, displaying significant growth inhibition at concentrations of 200 and 250 μg per disc, respectively.[54]

Chromatographic analysis of the organic extract of several isolates of *A. zeae* populations, obtained from several regions experiencing high temperatures and drought stress, confirmed the capacity of this fungus to produce both pyrrocidines A (**34**) and B (**14**) (Fig. 7).[55]

Further investigation by Wicklow and Poling of the organic extract from the maize-derived fungus *A. zeae* (obtained from the Agricultural Research Service Culture Collection) led to the isolation of the previously mentioned analogues **34** and **14**. Both compounds were evaluated for antimicrobial activity against a panel of maize pathogens and endophytes. Both analogues inhibited *A. flavus* and *F. verticillioides*, with compound **34** demonstrating superior potency to **14** (MIC ≤ 5 and ≤10 μM for **34** *vs.* >50 μM for **14**), relative to the positive control, nystatin (MIC ≤ 10 and ≤25 μM, respectively).

Additionally, pyrrocidine A (**34**) displayed significant antimicrobial activity (MIC = 1–2 μM) against several ear rot and stalk pathogens of maize, including *F. graminearum*, *N. oryzae*, *R. zeae*, and *S. maydis*. A notable inhibitory effect was also observed against *A. alternata* and *C. cladosporioides* (MIC = 5–10 μM), while a moderate effect was detected against *C. lunata* (MIC ≤ 10 μM); conversely, it was less effective against *T. viride* (MIC > 50 μM). Regarding pyrrocidine B (**14**), *N. oryzae* was the

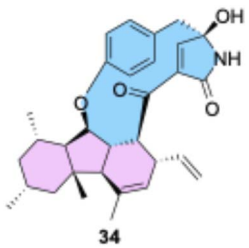

34

Fig. 7 Chemical structure of **34**.

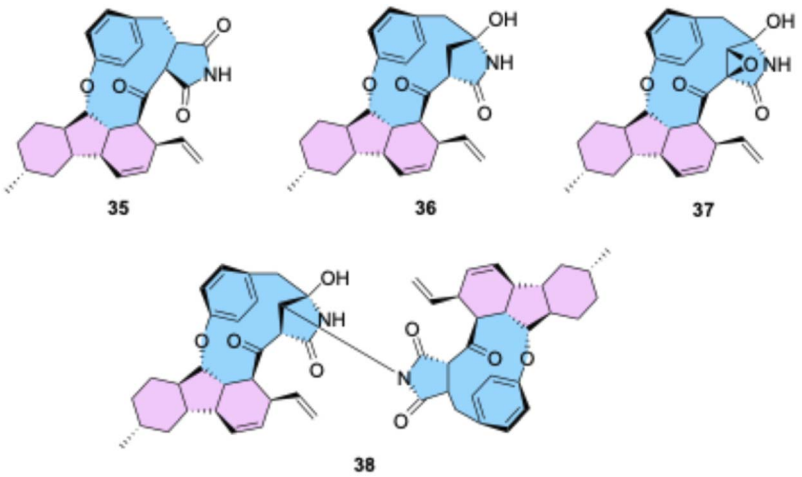

Fig. 8 Chemical structures of 35–38.

most sensitive strain tested, with an MIC value ranging between 5 and 10 μM.[56]

3.3.1.1.2. Fungi of the family Hypocreaceae. 3.3.1.1.2.1.Genus Trichoderma (*MycoBank ID 10282*) Chemical investigation of the endophyte-derived fungus *Trichoderma* sp., obtained from a decaying pod of *E. perseatha* collected in central Thailand, led to the isolation of three known alkaloid analogues, hirsutellones A–C (**35–37**), along with a novel alkaloid dimer, hirsutellone F (**38**) (Fig. 8). When evaluated for antitubercular activity against *Mycobacterium tuberculosis*, the alkaloid dimer **38** exhibited weak activity, with an MIC value of 3.12 μM. In comparison, compounds **35** and **36** displayed significantly stronger potency, both yielding MIC values of 0.78 μM. Conversely, when screened against *Plasmodium falciparum*, compound **38** showed a more pronounced inhibitory effect (IC_{50} = 4.2 μM) than compounds **35** and **36** (IC_{50} > 20 μM).[57]

3.3.1.1.3. Fungi of the family Nectriaceae. 3.3.1.1.3.1.Genus Neonectria (*MycoBank ID 234524*) Chemical investigation of the decayed-*branch*-derived fungus *N. ramulariae* led to the isolation of the previously mentioned polyketide alkaloid derivatives **13** and **34**, along with two novel analogues, pyrrospirones A (**39**) and B (**40**) (Fig. 9). All isolated compounds were evaluated for cytotoxic activity against HL-60, K562, and LNCaP cancer cell lines *via* the MTT assay. All tested derivatives exhibited significant cytotoxicity; the obtained IC_{50} values against the HL-60, K562, and LNCaP lines were 6.92, 8.64, and 11.74 μM for **13**, 0.12, 0.45, and 0.48 μM for **34**, 7.44, 9.27, and 20.24 μM for **39**, and 14.91, 9.96, and 17.97 μM for **40**, respectively. Additionally, at a concentration of 30 μM, pyrrospirones **39** and **40** induced apoptosis in HL-60 cancer cells.[58]

Further investigation of the same fungal strain by the research group led to the isolation of four additional previously undescribed derivatives: 17,18-epoxy-pyrrocidine B (**41**), 19-*O*-methyl-pyrrocidine B (**42**), 19-*O*-ethyl-pyrrocidine B (**43**), and alkaloid dimer bispyrrocidine (**44**) (Fig. 9). The isolated compounds were evaluated for cytotoxic activity against the HL-60 tumour cell line *via* the MTT assay. All four derivatives

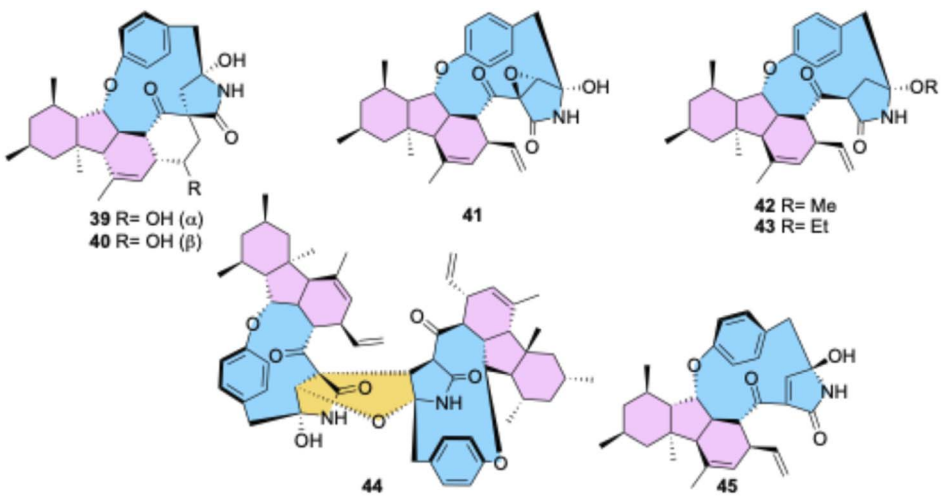

Fig. 9 Chemical structures of 39–45.

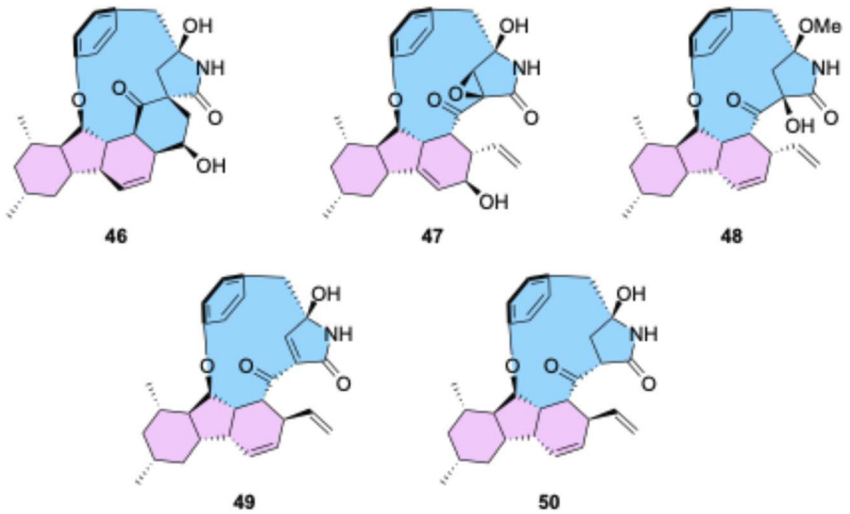

Fig. 10 Chemical structures of **46–50**.

exhibited weak cytotoxicity, displaying IC_{50} values of 4.6, 24.9, 15.1, and 22.2 μM, respectively, compared to the standard drug, adriamycin (IC_{50} = 0.02 μM). Additionally, the compounds were screened for their inhibitory effects on prolyl oligopeptidase activity. Among them, only alkaloid dimer **44** displayed moderate inhibition, with an IC_{50} value of 2.6 μM, while the remaining derivatives were inactive (IC_{50} > 10 μM), relative to the positive control, propeptin (IC_{50} = 1.1 μM).[59]

Further efforts by the same research group to elucidate the mode of action of pyrrocidine A (**34**) in suppressing the growth of HL-60 cells revealed that it induces caspase-dependent apoptosis. Additionally, its α,β-unsaturated carbonyl moiety exhibits high reactivity toward nucleophilic thiol groups. In conclusion, compound **34** represents a promising therapeutic candidate for the treatment of various malignancies.[60]

Chemical investigation of the insect-derived fungus *N. ramulariae*, isolated from the beetle *Holotrichia picea* collected in Yamagata Prefecture, Japan, led to the isolation of the previously mentioned pyrrocidine A (**34**), along with its novel derivative, 19-*epi*-pyrrocidine (**45**) (Fig. 9). Both compounds were evaluated for cytotoxic activity against the HL-60 cancer cell line. They displayed significant antiproliferative effects against the tested cells, yielding IC_{50} values of 0.12 and 2.05 μM, respectively.[61] Chemical investigation of the tropical plant-derived fungus *Cylindrocarpon* sp. (currently classified as *Neonectria* in the MycoBank database) led to the isolation of the previously mentioned analogues **34** and **42**. Both compounds were evaluated for cytotoxicity against A2780 tumour cells; only compound **34** displayed strong activity, yielding an IC_{50} value of 1.7 μM. Additionally, when screened for antibacterial activity against a panel comprising *Staphylococcus aureus* (ATCC 25923 and 700699), persistent *S. aureus* (ATCC 700699), *Enterococcus faecalis* (ATCC 29212 and 51299), and *Enterococcus faecium* (ATCC 35667 and 700221), the metabolites demonstrated strong to moderate inhibition. The observed MIC values ranged from 0.78 to 25 μM for 34 and from 25 to >100 μM for **42**, compared to the positive control, moxifloxacin.[62]

3.3.1.1.3.2. Genus Xenoacremonium (*MycoBank ID 810270*) Five previously undescribed alkaloid analogues, xenoacremones D–H (**46–50**) (Fig. 10), were recovered from the organic extract of the mangrove-derived fungus *Xenoacremonium sinensis*, which was isolated from *C. tagal* collected in Hainan Province, China. All isolated compounds were evaluated for their anti-inflammatory activity. While compound **49** was inactive (IC_{50} > 50 μM), the remaining derivatives (**46–48** and **50**) displayed weak to strong inhibitory activity against NO production, with IC_{50} values of 45.8, 37.5, 12.8, and 6.7 μM, respectively, compared to the positive control, resveratrol (IC_{50} = 36.0 μM). Additionally, the compounds were evaluated for cytotoxicity against NB4 and U937 tumour cell lines. Derivatives **46** and **48–50** exhibited weak to mild inhibitory activity, with IC_{50} values ranging between 6.4 and 18.4 μM. In contrast, compound **47** showed no effect (IC_{50} > 20 μM) relative to the positive control, adriamycin, which yielded IC_{50} values of 0.4 and 0.2 μM against the respective cell lines.[63] Furthermore, the structures of compounds **46–50** were revised by Novitskiy and Kutateladze (in 2022) *via in silico* studies.[64]

3.3.1.1.4. Fungi of the family Ophiocordycipitaceae. 3.3.1.1.4.1. Genus Hirsutella (*MycoBank ID 437737*) Chemical investigation of the insect-derived fungus *Hirsutella nivea*, obtained from a Homoptera leafhopper collected in Thailand, led to the isolation of the known analogues **35–37**, along with two novel derivatives, hirsutellones D (**51**) and E (**52**) (Fig. 11). Compounds **35–37** and **51** were evaluated for antimycobacterial activity against *Mycobacterium tuberculosis* H37Ra. They displayed weak to mild inhibitory activity, yielding MIC values of 0.78, 0.78, 0.78, and 3.125 μM, respectively, compared to the positive control, isoniazid (MIC = 0.06 μM). Additionally, the metabolites were screened for cytotoxicity against KB, BC, NCI-H187, and Vero cell lines. Compound **35** was inactive against all tested lines (IC_{50} > 20 and >50 μM), while analogues **36** and **51** were selectively active against NCI-H187 cells, with IC_{50} values of 6.0 and 7.3 μM, respectively. In contrast, compound **37**

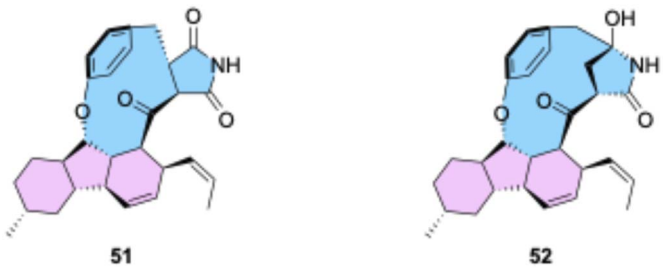

Fig. 11 Chemical structures of **51** and **52**.

proved to be the most potent cytotoxic agent, showing broad-spectrum activity with IC_{50} values of 4.6, 3.2, 8.3, and 12 μM against the respective cell lines.[65]

3.3.1.1.5. Fungi of the family Sarocladiaceae. 3.3.1.1.5.1. Genus Sarocladium (*MycoBank ID 519595*) The previously mentioned derivative **13** was isolated from the organic extract of *S. zeae*. Notably, *S. zeae* was found to modulate the secondary metabolic profile of competitor fungi, presumably serving as a pre-emptive mechanism for self-protection. This biocontrol capability holds significant potential for food safety applications by suppressing mycotoxin contamination.[66]

3.3.1.1.6. Fungi of unidentified family. 3.3.1.1.6.1.Genus Cephalosporium (*MycoBank ID 7525*) Chemical examination of the maize-derived fungus *Cephalosporium* sp. led to the detection of the previously mentioned analogues **13** and **34**. Both compounds were evaluated for antifungal activity against *F. verticillioides* and *A. flavus* using the paper disc method, displaying significant growth inhibition at 200 and 250 μg per disc, respectively.[54]

4. Structure–activity relationships (SARs)

Despite their substantial structural diversity, the 52 metabolites compiled here can be organised around a recurring architectural logic rather than a single strict chemotype. As summarised in Fig. 12, many members share three broad design features: a rigid polycyclic hydrophobic framework, an embedded amide/lactam polar module, and a set of peripheral substitution sites that absorb most of the observable molecular variation. This abstraction is useful for comparative discussion, but it should not be mistaken for a unified pharmacophore. The current compounds do not represent a single congeneric series interrogated under standardised biological conditions; rather, this review assembles structurally related fungal metabolites reported across different studies, organisms, and assay systems. Consequently, the analysis below should be read as a comparative structure–activity framework and not as a definitive SAR in the classical medicinal chemistry sense.

The compounds share the polycyclic core as an organisational element. Its contribution is unlikely to be target-specific in any narrow sense; rather, it appears to be a privileged natural-product scaffold that combines a high hydrophobic surface area with pronounced conformational restriction. Such a profile is often compatible with whole-cell activity, particularly in the antibacterial phenotypic space, where membrane partitioning and reduced entropic penalties can promote detectable activity. However, this same physicochemical signature also poses an immediate interpretive problem, as it is equally compatible with nonspecific membrane association, promiscuous target engagement and cytotoxicity. The prevalence of co-occurring antibacterial and cytotoxic annotations amongst the more lipophilic members of the series suggests that the scaffold may favour broad cellular activity at least as much as selective pharmacology. In other words, the core may be necessary for bioactivity, but it is unlikely to be sufficient to explain functional selectivity.

The amide/lactam motif is one of the few polar interaction moieties that is conserved across otherwise diverse scaffolds and is therefore the most likely candidate for a recurrent recognition feature. Its occurrence in several subfamilies suggests a major role in maintaining a basal level of polarity and hydrogen-bonding capability in a very hydrophobic environment. Yet, caution is called for. Conservation of a lactam or an amide does not imply conservation of the binding mode, molecular target or mechanism of action. At this level of

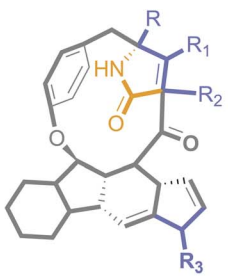

Drive 3D shape and hydrophobic surface area, supporting cell penetration and contributing to multiple activity classes.

The amide/lactam carbonyl and NH provide H-bonding features that can support target engagement across activity classes.

Polar and small substituents are beneficial for anti-inflammatory activity.

Bulky and hydrophobic substituents are beneficial for cytotoxicity and antibacterial activities.

Fig. 12 Generalised scaffold and SAR hotspots.

analysis, it is more defensible to view the motif as a reusable interaction handle rather than as evidence for a shared pharmacological mechanism.

Most of the observed SARs seem to be mediated by substitution at the periphery. The variation at R and R1–R3 likely tunes the balance between lipophilicity and polarity, and along with this, the probability that a given scaffold will occupy the antibacterial/cytotoxic *versus* anti-inflammatory/antimalarial activity space. Among the collected compounds, metabolites in the mid-to-high lipophilicity regime ($c\log P \approx 4$–6) are more frequently associated with antibacterial and cytotoxic annotations, whereas more oxygenated and less lipophilic congeners are more frequently associated with anti-inflammatory or antimalarial readouts.[42] This trend is chemically consistent, but its significance is not simple. In fact, higher $c\log P$ could be beneficial to whole-cell potency by increasing the affinity to the membrane and intracellular exposure, but it could also simply magnify nonspecific interactions and inflate apparent activity in phenotypic assays.[67] This second interpretation is a serious competing explanation that cannot be ignored in light of the persistent overlap between antibacterial and cytotoxic behaviours.

The reverse direction of this trend, *i.e.*, preferential association of more polarity-balanced analogues with anti-inflammatory and antimalarial annotations, is also interesting, but should not be overinterpreted. Compounds within the xenoacremone and hirsutellone families indicate that reduced lipophilicity and enhanced oxygenation may help to modulate behaviour away from overly cytotoxic phenotypes to more differentiated bioactivity. However, the current evidence does not clarify if this is due to better target selectivity, altered uptake, different intracellular distributions or just the fact that different scaffold subclasses were tested for different endpoints. This is a key distinction. Much of what looks like SARs in heterogeneous natural product datasets is actually an overlay of the assay bias, chemotype bias and taxonomic bias.

Fig. 12 provides a useful conceptual model for future optimisation, but does not provide a predictive SAR map. The most defensible conclusion is that peripheral decoration modulates the exposure-polarity landscape imposed on a relatively conserved rigid core and that this modulation affects whether compounds fall into a more broadly bioactive, lipophilicity-driven region of chemical space or into a somewhat more polarity-balanced region associated with anti-inflammatory and antimalarial annotations. However, it remains to be seen whether these trends are true mechanism-linked SARs, which can only be determined by matched analogue series, standardised cross-assay testing and direct selectivity measurements. Until then, the current framework should be considered hypothesis-generating rather than rule-defining.

5. Pharmacokinetics, ADMET and druglikeness properties

Here, we assembled 52 pyrrocidines and hirsutellones from 18 fungal genera that occupy a biologically attractive yet developmentally challenging region of chemical space. Reported activities include cytotoxic, antibacterial, antimalarial, antifungal, and anti-inflammatory effects, highlighting the functional diversity of these compounds. However, this very diversity makes a simple physicochemical interpretation difficult. Because these compounds were not generated in a coordinated optimisation campaign but rather collated from different studies, their ADMET descriptors are best viewed as a landscape of developability constraints and opportunities, rather than as a basis for simple lead-likeness ranking. Accordingly, the drug-like characteristics of these 52 compounds (Fig. 13, Table S1, SI) were assessed using the RDKit software.[68]

At the broadest level, these metabolites occupy a recognisable natural-product domain characterised by a relatively high molecular weight, moderate-to-high lipophilicity, low conformational flexibility, and variable but often substantial polarity. Many clusters are ~480–560 Da, consistent with a shared biosynthetic preference for compact, polycyclic terpene-polyketide architectures. This clustering supports the view that several subfamilies arise from related structural logic, but it does not by itself confer favourable developability. Indeed, compounds near or beyond this mass range already sit at the margins of conventional small-molecule design, where permeability, solubility, and formulation constraints often become intertwined.

The high-molecular-weight outliers are especially informative. Species such as bispyrrocidine, hirsutellone F, didymellanosine, and penicillione F demonstrate that fungal secondary metabolism can readily generate structures extending toward ~700–1000 Da through dimerization or extensive functionalisation. These compounds expand the chemical imagination of the class, but they also expose a practical limitation of descriptor-based summarisation: a few extreme metabolites can materially broaden the apparent property space without necessarily yielding a transferable medicinal chemistry strategy. Their presence is therefore important less because they define the class, and more because they reveal its outer boundaries.

Lipophilicity provides one of the clearest axes of differentiation across the dataset. A substantial fraction of metabolites occupies the $c\log P$ range of ~4–6, while others shift toward lower values or extend into a markedly lipophilic space above 7. This dispersion almost certainly reflects differences in the oxidation state, peripheral carbon density, and scaffold elaboration rather than changes in the underlying polycyclic framework alone. Notably, several compounds in the more lipophilic region, including penicipyrrodiether A and ascomylactam B, are associated with cytotoxic activity. While this observation is often taken as indirect support for improved cellular uptake, such an interpretation is incomplete unless paired with its toxicological corollary: high lipophilicity also increases the likelihood of membrane perturbation, off-target binding, and reduced selectivity. Thus, the apparent enrichment of antibacterial and cytotoxic annotations among more lipophilic metabolites may signify a generalised whole-cell exposure advantage, but not necessarily a therapeutically useful activity profile.

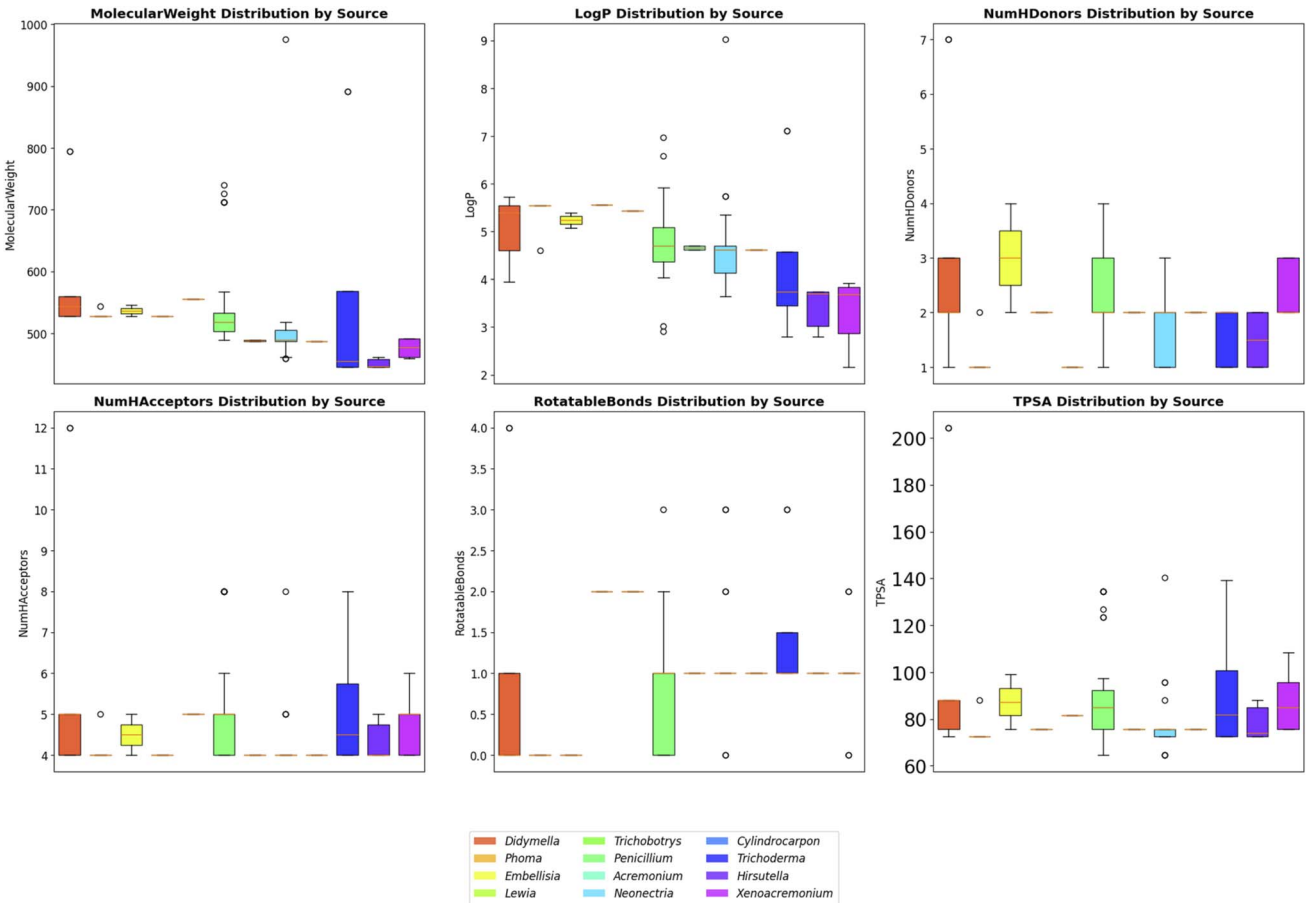

Fig. 13 Distribution of the molecular weight (MW), calculated octanol–water partition coefficient ($c\log P$), number of acceptor groups (acceptors), number of donor groups (donors), number of rotatable bonds and topological polar surface area (TPSA) by fungal genera (*Penicillium*, *Neonectria*, *Didymella*, *Xenoacremonium*, *Trichoderma*, *Phoma*, *Hirsutella*, *Embellisia*, *Acremonium*, *Lewia*, *Trichobotrys*, and *Cylindrocarpon*).

By contrast, the lower-lipophilicity region contains several compounds annotated as anti-inflammatory or antimalarial, including members of the xenoacremone and hirsutellone series. This pattern is consistent with the possibility that more balanced polarity supports more differentiated biological behaviour, perhaps by reducing membrane-driven promiscuity or by improving the balance between aqueous solubility and cellular exposure. However, such a reading remains provisional. Without matched potency, selectivity, and permeability data, it is not possible to determine whether a lower $c\log P$ is mechanistically beneficial or merely correlated with particular scaffold families and assay histories. This caveat is especially important in review-level interpretation because cross-class physicochemical trends can otherwise be mistaken for actionable medicinal chemistry principles.

Polarity descriptors reinforce this ambiguity. Most compounds cluster in a moderate band of hydrogen-bonding capacity and TPSAs (~70–100 Å^2), but a subset extends to far higher polarity. These high-polarity outliers are especially valuable because they challenge standard assumptions about passive permeability and oral drug-likeness. Didymellanosine, for example, with a TPSA of ~204 Å^2, lies well outside the descriptor space typically associated with efficient passive diffusion. Its inclusion highlights a central tension in fungal natural-product discovery: biologically active metabolites can reside far beyond the conventional lead-like space, yet their activity may depend on transport processes, intracellular accumulation patterns, or assay environments that are difficult to leverage in downstream optimisation. In that sense, apparent bioactivity does not necessarily translate into tractable pharmacology.

Low rotatable bond counts across most of the dataset confirm that conformational rigidity is a defining feature of the class. This rigidity may be advantageous for binding efficiency by lowering entropic penalties and preserving the three-dimensional shape. At the same time, its value should not be romanticised. In molecules that are already large and lipophilic, rigidity can coexist with substantial developability liabilities and may leave limited room for property correction without destabilising the core architecture. Thus, what is often celebrated as structural preorganisation may, from a medicinal chemistry perspective, also represent restricted optimisation latitude.

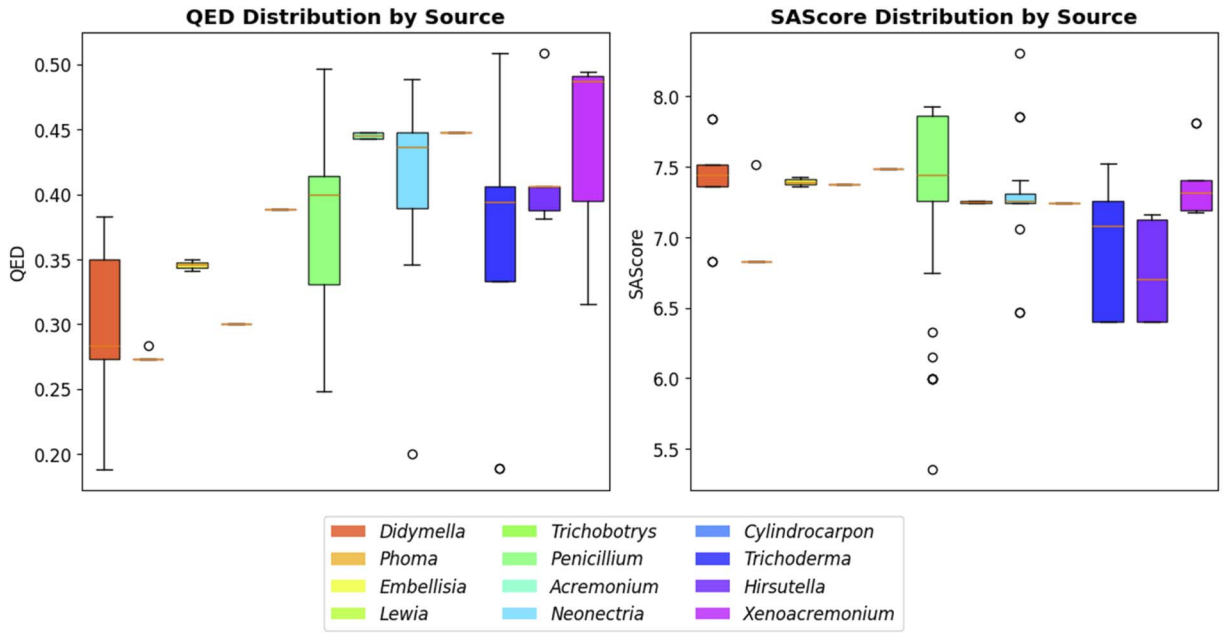

Fig. 14 Distribution of the quantitative estimation of drug-likeness (QED) and synthetic accessibility (SA) score by fungal genera (*Penicillium*, *Neonectria*, *Didymella*, *Xenoacremonium*, *Trichoderma*, *Phoma*, *Hirsutella*, *Embellisia*, *Acremonium*, *Lewia*, *Trichobotrys*, and *Cylindrocarpon*).

The QED and SA analyses (Fig. 14) sharpen this picture further. Moderate-to-low QED values (~0.2–0.5) and relatively high SA scores (~6–8) indicate that these metabolites are unlikely to behave as straightforward lead-like molecules under conventional drug design criteria. Yet, it would be reductive to interpret this as evidence of poor value. Rather, these metrics expose a deeper and familiar paradox of natural-product discovery: the same features that generate structural novelty and potent phenotypic activity, polycyclic rigidity, stereochemical density, and scaffold complexity also create barriers to synthesis, analogue expansion, solubility optimisation, and property control. In this class, poor "drug-likeness" is not a verdict against biological relevance; it is a warning that translation into a tractable programme will require unusually deliberate chemistry.

6. Conclusion and future perspectives

For decades, natural products have provided medicine with an invaluable platform of safe and highly effective therapeutic agents across diverse clinical fields. Fungi, a highly diverse kingdom of eukaryotic organisms, inhabit a wide range of environments and are associated with various marine and terrestrial hosts. Throughout history, they have also played a vital role in traditional medicine. Recently, increasing attention has been directed toward fungi as a prolific reservoir of pharmacologically active metabolites with significant potential in drug discovery. In this review, we have presented a comprehensive analysis of the biosynthetic pathways and an up-to-date survey of pyrrocidines and hirsutellones isolated from fungal sources between 2005 and 2025. A total of 52 structurally diverse pyrrocidines and hirsutellones derived from various fungal genera have been documented and discussed, accompanied by an exploration of their structure–activity relationships as well as an extensive analysis of their pharmacokinetics, ADMET, and drug-likeness properties.

Furthermore, an analysis of the taxonomic distribution of pyrrocidine and hirsutellone metabolites at higher fungal ranks reveals a clear concentration within three major ascomycete classes, reflecting both biosynthetic specialization and research focus (Fig. 15). Sordariomycetes represent the largest contributing class, accounting for 24 compounds (42%), all of which fall within the subclass Hypocreomycetidae and the order Hypocreales. Eurotiomycetes constitute the second most significant group, contributing 22 compounds (39%) exclusively assigned to the subclass Eurotiomycetidae and the order Eurotiales. In contrast, Dothideomycetes account for a smaller yet notable portion of the dataset, with 11 compounds (19%) distributed entirely within the subclass Pleosporomycetidae and the order Pleosporales.

Collectively, this distribution demonstrates that pyrrocidines and hirsutellones are not restricted to a single evolutionary lineage but are concentrated in specific ascomycete clades with well-developed secondary metabolic machinery. The dominance of Hypocreales and Eurotiales further suggests that these orders represent particularly fertile sources for pyrrocidines, hirsutellones, and other PKS-NRPS hybrid metabolites, potentially warranting prioritized investigation in future natural product discovery efforts.

An evaluation of the family-level distribution of pyrrocidine and hirsutellone metabolites highlights a pronounced concentration within a small number of ascomycete families, reflecting both biosynthetic capacity and taxonomic trends in secondary

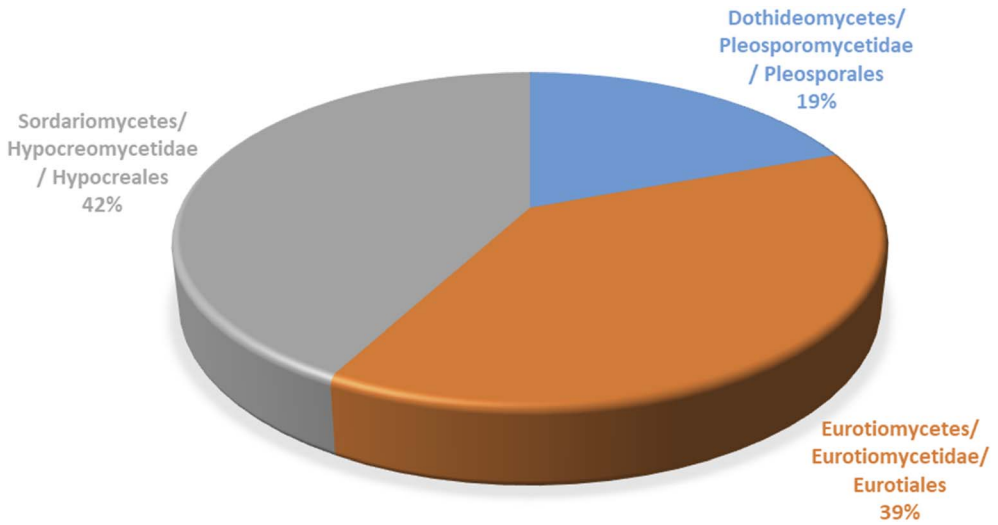

Fig. 15 Contribution of pyrrocidines and hirsutellones by different fungal classes, subclasses and orders.

metabolism (Fig. 16). Aspergillaceae is the dominant family, with 22 compounds, all of which are produced by the genus *Penicillium*, reflecting its exceptional capacity for generating PKS-NRPS-derived metabolites. Nectriaceae represents the second most significant family, with 14 compounds. Furthermore, members of the Didymellaceae family contribute 7 compounds. Notably, the family Ophiocordycipitaceae accounts for 5 compounds, whereas Bionectriaceae and Hypocreaceae each account for 4 compounds. Smaller contributions are observed from the families Pleosporaceae (3 compounds) and Sarocladiaceae (1 compound). Additionally, 2 compounds are derived from unidentified taxa classified at the genus level as *Cephalosporium*. Collectively, this family-level distribution shows that pyrrocidines and hirsutellones are concentrated within families with robust secondary metabolic pathways, while their presence across multiple families reveals the evolutionary dissemination and biosynthetic versatility of this metabolic scaffold.

Based on the compiled dataset of pyrrocidine and hirsutellone metabolites (52 derivatives collectively), the distribution across fungal genera shows a clear dominance of a limited number of taxonomic groups, alongside contributions from several less-represented genera (Fig. 17). Remarkably, *Penicillium* emerges as the most prolific source, accounting for 22 metabolites, which underlines its well-known capacity for secondary metabolite biosynthesis and chemical diversification. This is followed by *Neonectria*, from which 9 metabolites have been reported, highlighting its consistent contribution to

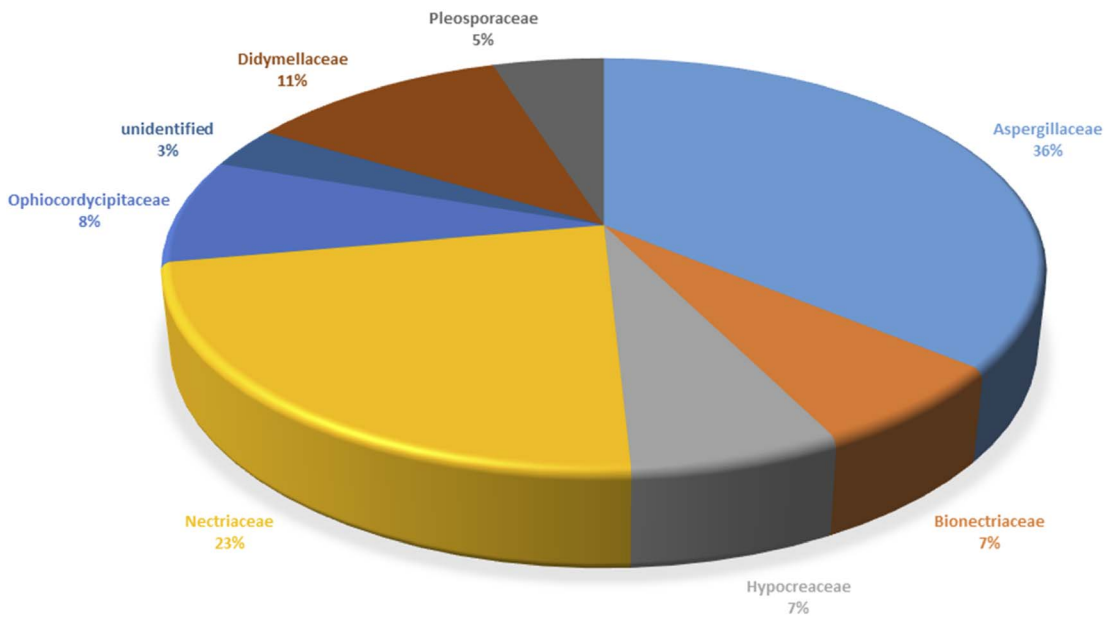

Fig. 16 Contribution of pyrrocidines and hirsutellones by different fungal families.

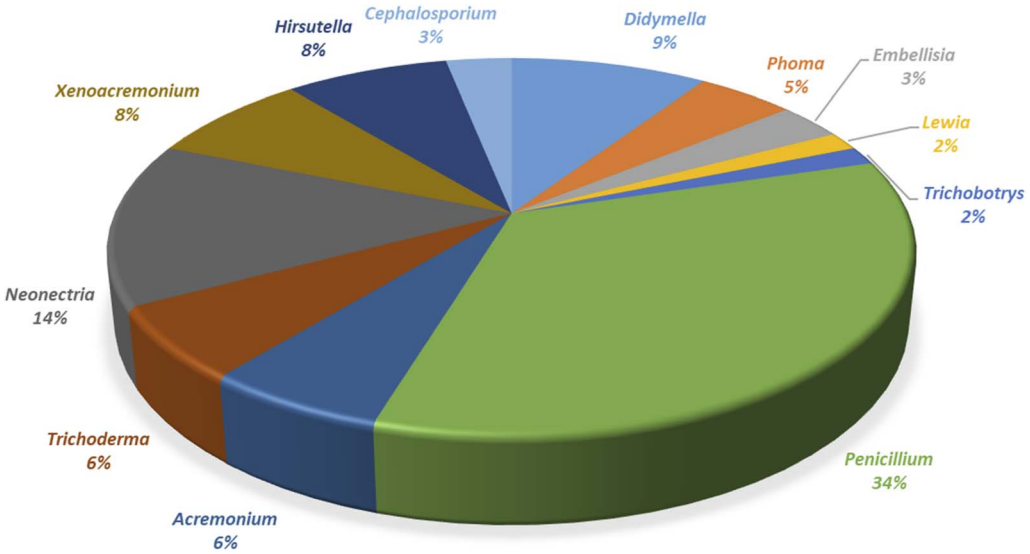

Fig. 17 Contribution of pyrrocidines and hirsutellones by different fungal genera.

this scaffold family. Moderate numbers of metabolites have been isolated from *Didymella* (6), *Xenoacremonium* (5), and *Hirsutella* (5), reflecting a broader but still focused taxonomic spread. Furthermore, *Acremonium* and *Trichoderma* each contribute 4 metabolites, while *Phoma* (3), *Embellisia* (2), and *Cephalosporium* (2) represent smaller yet notable sources. In contrast, *Lewia*, *Trichobotrys*, and *Sarocladium* each have a single reported metabolite, suggesting either limited biosynthetic output or underexplored genera. Collectively, this distribution highlights both the central role of *Penicillium* species in shaping the chemical landscape of pyrrocidines and hirsutellones and the broader evolutionary dissemination of this scaffold across phylogenetically diverse fungi, reinforcing its biosynthetic robustness and relevance for natural product discovery.

The biological activity profile of pyrrocidines and hirsutellones is strongly skewed toward cytotoxic and antibacterial activities, reflecting both scaffold potency and historical research emphasis (Fig. 18). Across the reviewed dataset, 39 derivatives exhibit cytotoxic activity, underscoring their relevance to anticancer research, while 21 display antibacterial activity, consistent with their ecological role in microbial competition. In contrast, alternative bioactivities are less frequently reported, including antifungal (5 compounds), anti-inflammatory (4 compounds), and antimalarial (3 compounds) properties. Enzyme inhibition and phytotoxicity have been observed for only 1 compound each, suggesting that these chemical spaces remain largely underexplored. Overall, this distribution highlights a strong focus on cytotoxic and antibacterial screening while indicating clear opportunities for a broader biological evaluation of this metabolite family.

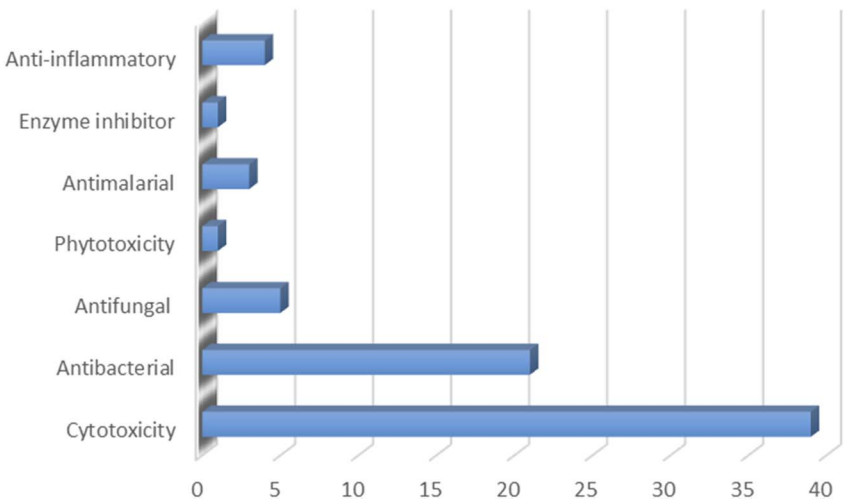

Fig. 18 Therapeutic activities of different pyrrocidines and hirsutellones obtained from various fungal species.

7. Author contributions

Conceptualization: Amr El-Demerdash and Mohamed A. Tammam. Validation: Mohamed A. Tammam and Amr El-Demerdash. Formal analysis: Mohamed A. Tammam, Islam El-Awaad, Adnane Aouidate and Amr El-Demerdash. Investigation: Mohamed A. Tammam, Islam El-Awaad, Adnane Aouidate and Amr El-Demerdash. Resources: Mohamed A. Tammam, Islam El-Awaad, Adnane Aouidate, Reham Hassan Mekky and Amr El-Demerdash. Data curation: Mohamed A. Tammam and Amr El-Demerdash. Writing – original draft: Mohamed A. Tammam, Islam El-Awaad, Adnane Aouidate, Reham Hassan Mekky and Amr El-Demerdash. Writing – review and editing: Mohamed A. Tammam, Islam El-Awaad, Adnane Aouidate, Reham Hassan Meeky and Amr El-Demerdash.

8. Conflicts of interest

There are no conflicts to declare.

9. Abbreviations

A	Adenylation domain
A2780	Human ovarian cancer cell line
A549	Human nonsmall cell lung carcinoma
ACP	Acyl carrier protein
AT	Acyltransferase
C	Condensation domain
Colo-320	Human colorectal cancer cell line
DH	Dehydratase
DOX	Doxorubicin
EPI	Epirubicin
ER	Enoyl reductase
Glioma SHG-44	Shenyang human glioma-clone 44
Glioma U251	U-251 glioblastoma multiforme
Glioma U87-MG	Uppsala 87 malignant glioma
HCT116	Colon cancer cell line
HeLa S3	Subclone of the original HeLa cell line
HP	Hypothetical protein
IMDA	Intramolecular Diels–Alder
Jurkat	Human T lymphocyte (T-cell) leukaemia
Jurkat J16	Adult lymphoblastic leukaemia T cells
K562	Human chronic myelogenous leukaemia
KB	Cervical uterine cancer
KR	Ketoreductase
KS	Ketosynthase
L5178Y	Murine lymphoma cell line
LC-HRMS	Liquid chromatography-high-resolution mass spectrometry
LLP	Lipocalin-like protein
LNCaP	Human prostate carcinoma
LORA	Low oxygen recovery assay
MABA	Microplate alamar blue assay
MDA-MB-231	Human breast cancer cell line
MDA-MB-435	Human melanoma cell line
MDA-MB-435	Metastatic melanoma
MDR	Medium-chain dehydrogenase reductase
MIC	Minimum inhibition concentration
MRC5	Non-malignant human fatal lung fibroblast
MT	Methyl transferase
MTT method	Colorimetric assay for assessing cell metabolic activity
NCI-H460	Lung carcinoma
PBMC	Noncancerous peripheral blood mononuclear cells
PC-3	Prostatic cancer
PKS-NRPS	Polyketide synthase-nonribosomal peptide synthetase
R	Terminal reductase domain
Ramos	Burkitt's lymphoma B cells
SAM	*S*-adenosyl methionine
SNB19	Human glioblastoma cell line
T	Thiolation domain
trans-ER	*Trans*-enoyl reductase
U251	Human glioblastoma multiforme

10. Data availability

This is a review article. No primary research results, software or code have been included, and no new data were generated or analysed as part of this review.

Supplementary information (SI): the word file: list of 52 recorded pyrrocidines, hirsutellones and related congeners; the spreed sheet: the drug-like characteristics of these 52 compounds. See DOI: https://doi.org/10.1039/d6np00044d.

11. Acknowledgements

Amr El-Demerdash is thankful to his home universities, the University of East Anglia (UK) and Mansoura University (Egypt), for the unlimited support, inside and outside. Mohamed A. Tammam is humbly dedicating this work to the soul of his sister Dr Mai A. Tammam who passed away on 19 March 2022, and was always a kind supporter in all aspects of his life.

12. References

1 G. M. Cragg and D. J. Newman, *Pure Appl. Chem.*, 2005, **77**, 7–24.
2 M. A. Tammam, F. Pereira, E. Skellam, S. Bidula, A. Ganesan and A. El-Demerdash, *Nat. Prod. Rep.*, 2025, **42**, 788–841.
3 M. S. Butler and J. J. La Clair, *J. Nat. Prod.*, 2025, **89**, 3–28.
4 R. H. Mekky, M. E. Abo-El Fetoh, S. A. Faheem, A. F. Radwan, M. H. Fawzy, A. M. Mustafa, M. A. Said, D. Calina, J. Sharifi-Rad and W. C. Cho, *MedComm*, 2025, **6**, e70278.
5 M. A. Tammam, M. I. Gamal El-Din, A. Aouidate and A. El-Demerdash, *Bioorg. Chem.*, 2024, 107654.
6 S. Gagare, P. Patil and A. Jain, *J. Pharm. Sci.*, 2024, **10**(1), 55.

7 A. G. Atanasov, S. B. Zotchev, V. M. Dirsch, I. E. Orhan, M. Banach, J. M. Rollinger, D. Barreca, W. Weckwerth, R. Bauer, E. A. Bayer, M. Majeed, A. Bishayee, V. Bochkov, G. K. Bonn, N. Braidy, F. Bucar, A. Cifuentes, G. D'Onofrio, M. Bodkin, M. Diederich, A. T. Dinkova-Kostova, T. Efferth, K. El Bairi, N. Arkells, T. P. Fan, B. L. Fiebich, M. Freissmuth, M. I. Georgiev, S. Gibbons, K. M. Godfrey, C. W. Gruber, J. Heer, L. A. Huber, E. Ibanez, A. Kijjoa, A. K. Kiss, A. Lu, F. A. Macias, M. J. S. Miller, A. Mocan, R. Müller, F. Nicoletti, G. Perry, V. Pittalà, L. Rastrelli, M. Ristow, G. L. Russo, A. S. Silva, D. Schuster, H. Sheridan, K. Skalicka-Woźniak, L. Skaltsounis, E. Sobarzo-Sánchez, D. S. Bredt, H. Stuppner, A. Sureda, N. T. Tzvetkov, R. A. Vacca, B. B. Aggarwal, M. Battino, F. Giampieri, M. Wink, J. L. Wolfender, J. Xiao, A. W. K. Yeung, G. Lizard, M. A. Popp, M. Heinrich, I. Berindan-Neagoe, M. Stadler, M. Daglia, R. Verpoorte and C. T. Supuran, *Nat. Rev. Drug Discovery*, 2021, **20**, 200–216.

8 A. S. Abdel-Razek, M. E. El-Naggar, A. Allam, O. M. Morsy and S. I. Othman, *Processes*, 2020, **8**, 470.

9 M. A. Tammam, M. I. Gamal El-Din, A. Abood and A. El-Demerdash, *RSC Adv.*, 2023, **13**, 8049–8089.

10 D. Jakubczyk and F. Dussart, *Molecules*, 2020, **25**, 911.

11 E. A. Elsayed, H. El Enshasy, M. A. M. Wadaan and R. Aziz, *Mediators Inflammation*, 2014, **2014**, 805841.

12 J. Xu, M. Yi, L. Ding, S. He, L. Dak, S. Yip, Y. Chin and K. Li, *Mar. Drugs*, 2019, **17**, 636.

13 V. V. Pandey, V. K. Varshney and A. Pandey, *J. Biol. Act. Prod. Nat.*, 2019, **9**, 162–178.

14 S. K. Deshmukh, V. Prakash and N. Ranjan, *Front. Microbiol.*, 2018, **8**, 2536.

15 A. Ganjoo, N. Sharma, H. Shafeeq, N. A. Bhat, K. K. Dubey and V. Babu, *Biotechnol. Bioeng.*, 2022, **119**, 3339–3369.

16 J. Correia, A. Borges, M. Simões and L. C. Simões, *Antibiotics*, 2023, **12**, 1250.

17 M. A. Tammam, M. Sebak, C. Greco, A. Kijjoa and A. El-Demerdash, *J. Mol. Struct.*, 2022, **1268**, 133711.

18 M. Sebak, F. Molham, C. Greco, M. A. Tammam, M. Sobeh and A. El-Demerdash, *RSC Adv.*, 2022, **12**, 24887–24921.

19 A. El-Demerdash, *J. Fungi*, 2018, **4**, 130.

20 X. W. Li, A. Ear and B. Nay, *Nat. Prod. Rep.*, 2013, **30**, 765–782.

21 K. C. Nicolaou, D. Sarlah, T. Robert Wu and W. Zhan, *Angew. Chem., Int. Ed.*, 2009, **48**, 6870–6874.

22 M. Ohashi, T. B. Kakule, M. C. Tang, C. S. Jamieson, M. Liu, Y. L. Zhao, K. N. Houk and Y. Tang, *J. Am. Chem. Soc.*, 2021, **143**, 5605–5609.

23 B. Nay, M. Zaghouani, B. Laroche, S. Prévost, X. W. Li, A. Ear and N. Riache, *Strategies Tactics Org. Synth.*, 2017, **13**, 55–80.

24 N. Riache, I. Ndoye, X. W. Li and B. Nay, *Synlett*, 2011, **2011**, 2685–2688.

25 K. P. Reber, S. D. Tilley, C. A. Carson and E. J. Sorensen, *J. Org. Chem.*, 2013, **78**, 9584–9607.

26 Q. Yin, X. Liu, Z. Zhang, H. Lei and B. Wu, *Fitoterapia*, 2023, **164**, 105377.

27 H. Oikawa, *J. Org. Chem.*, 2003, **68**, 3552–3557.

28 A. Ear, S. Amand, F. Blanchard, A. Blond, L. Dubost, D. Buisson and B. Nay, *Org. Biomol. Chem.*, 2015, **13**, 3662–3666.

29 C. Y. Chiang, M. Ohashi and Y. Tang, *Nat. Prod. Rep.*, 2023, **40**, 89–127.

30 Y. Chen, S. Sewsurn, S. Amand, C. Kunz, N. Pietrancosta, K. Calabro, D. Buisson and S. Mann, *ACS Chem. Biol.*, 2024, **19**, 886–895.

31 Z. Liu, W. Li, P. Zhang, J. Fan, F. Zhang, C. Wang, S. Li, Y. Sun, S. Chen and W. Yin, *Acta Pharm. Sin. B*, 2021, **11**, 3655–3664.

32 Y. Chen, *Deciphering the biosynthetic pathways of PKS-NRPS derived metabolites from the endophytic fungus Sarocladium zeae : Elucidation of pyrrocidines biosynthesis*, Organic chemistry, Sorbonne Université, 2022, English, NNT : 2022SORUS133, DOI: 10.70675/683D2176ZF163Z499BZ8C95Z6CE34449FBC6.

33 B. S. Jeon, S. A. Wang, M. W. Ruszczycky and H. W. Liu, *Chem. Rev.*, 2016, **117**, 5367–5388.

34 B. Zhang and H. M. Ge, *Natl. Sci. Rev.*, 2022, **11**, nwac229.

35 L. Gao, C. Su, X. Du, R. Wang, S. Chen, Y. Zhou, C. Liu, X. Liu, R. Tian, L. Zhang, K. Xie, S. Chen, Q. Guo, L. Guo, Y. Hano, M. Shimazaki, A. Minami, H. Oikawa, N. Huang, K. N. Houk, L. Huang, J. Dai and X. Lei, *Nat. Chem.*, 2020, **12**, 620–628.

36 Y. Cai, Y. Hai, M. Ohashi, C. S. Jamieson, M. Garcia-Borras, K. N. Houk, J. Zhou and Y. Tang, *Nat. Chem.*, 2019, **11**, 812–820.

37 H. J. Kim, M. W. Ruszczycky, S. H. Choi, Y. N. Liu and H. W. Liu, *Nature*, 2011, **473**, 109–112.

38 N. Kato, T. Nogawa, H. Hirota, J. H. Jang, S. Takahashi, J. S. Ahn and H. Osada, *Biochem. Biophys. Res. Commun.*, 2015, **460**, 210–215.

39 M. Sato, S. Kishimoto, M. Yokoyama, C. S. Jamieson, K. Narita, N. Maeda, K. Hara, H. Hashimoto, Y. Tsunematsu, K. N. Houk, Y. Tang and K. Watanabe, *Nat. Catal.*, 2021, **4**, 223–232.

40 M. Sato, F. Yagishita, T. Mino, N. Uchiyama, A. Patel, Y. H. Chooi, Y. Goda, W. Xu, H. Noguchi, T. Yamamoto, K. Hotta, K. N. Houk, Y. Tang and K. Watanabe, *ChemBioChem*, 2015, **16**, 2294–2298.

41 Y. Chen, Z. Liu, Y. Huang, L. Liu, J. He, L. Wang, J. Yuan and Z. She, *J. Nat. Prod.*, 2019, **82**, 1752–1758.

42 N. P. Ariantari, E. Ancheeva, M. Frank, F. Stuhldreier, D. Meier, Y. Gröner, I. Reimche, N. Teusch, S. Wesselborg, W. E. G. Müller, R. Kalscheuer, Z. Liu and P. Proksch, *RSC Adv.*, 2020, **10**, 7232–7240.

43 E. M. K. Wijeratne, H. He, S. G. Franzblau, A. M. Hoffman and A. A. L. Gunatilaka, *J. Nat. Prod.*, 2013, **76**, 1860–1865.

44 W. Ebrahim, A. H. Aly, V. Wray, A. Mándi, M. H. Teiten, F. Gaascht, B. Orlikova, M. U. Kassack, W. Lin, M. Diederich, T. Kurtán, A. Debbab and P. Proksch, *J. Med. Chem.*, 2013, **56**, 2991–2999.

45 T. M. Casella, V. Eparvier, H. Mandavid, A. Bendelac, G. Odonne, L. Dayan, C. Duplais, L. S. Espindola and D. Stien, *Phytochemistry*, 2013, **96**, 370–377.

46 S. Chen, H. Shen, P. Zhang, H. Cheng, X. Dai and L. Liu, *Chem. Commun.*, 2019, **55**, 1438–1441.
47 J. Becker, J. C. Liermann, T. Opatz, H. Anke and E. Thines, *J. Antibiot.*, 2012, **65**, 99–102.
48 T. Song, M. Chen, Z. W. Ge, W. Chai, X. C. Li, Z. Zhang and X. Y. Lian, *J. Org. Chem.*, 2018, **83**, 13395–13401.
49 T. Song, M. Chen, W. Chai, Z. Zhang and X. Y. Lian, *Tetrahedron*, 2018, **74**, 884–891.
50 T. Song, M. Tang, H. Ge, M. Chen, X. Lian and Z. Zhang, *Mar. Drugs*, 2019, **17**, 292.
51 X. Qi, X. Li, J. Zhao, N. He, Y. Li, T. Zhang, S. Wang, L. Yu and Y. Xie, *J. Antibiot.*, 2019, **72**, 237–240.
52 N. Liu, M. N. Song, Q. Q. Zhang, C. Wu, K. K. Zhu, Y. L. Sun, M. R. Li, F. Y. Yang, R. L. Feng, Y. Y. Zhang and H. Zhang, *Chin. J. Nat. Med.*, 2022, **20**, 67–73.
53 Y. Ding, Y. Jiang, S. Xu, X. Xin and F. An, *Chin. Chem. Lett.*, 2023, **34**, 107562.
54 D. T. Wicklow, S. Roth, S. T. Deyrup and J. B. Gloer, *Mycol. Res.*, 2005, **109**, 610–618.
55 D. T. Wicklow, S. M. Poling and R. C. Summerbell, *Can. J. Plant Pathol.*, 2008, **30**, 425–433.
56 D. T. Wicklow and S. M. Poling, *Phytopathology*, 2008, **99**, 109–115.
57 M. Isaka, W. Prathumpai, P. Wongsa and M. Tanticharoen, *Org. Lett.*, 2006, **8**, 2815–2817.
58 Y. Shiono, K. Shimanuki, F. Hiramatsu, T. Koseki, M. Tetsuya, N. Fujisawa and K. ichi Kimura, *Bioorg. Med. Chem. Lett.*, 2008, **18**, 6050–6053.
59 Y. Shiono, A. Kosukegawa, T. Koseki, T. Murayama, E. Kwon, S. Uesugi and K. I. Kimura, *Phytochem. Lett.*, 2012, **5**, 91–95.
60 S. Uesugi, N. Fujisawa, J. Yoshida, M. Watanabe, S. Dan, T. Yamori, Y. Shiono and K. I. Kimura, *J. Antibiot.*, 2015, **69**, 133–140.
61 Y. Shiono, M. Furukawa, T. Koseki, E. Kwon, A. H. Kurniawan, S. Sato, D. Harneti, R. Maharani, U. Supratman, S. Uesugi and K. ichi Kimura, *Phytochem. Lett.*, 2018, **26**, 120–124.
62 R. S. T. Kamdem, W. Pascal, N. Rehberg, L. van Geelen, S. P. Höfert, T. O. Knedel, C. Janiak, P. Sureechatchaiyan, M. U. Kassack, W. Lin, R. Kalscheuer, Z. Liu and P. Proksch, *Fitoterapia*, 2018, **128**, 175–179.
63 Z. Liu, L. Liu, A. Wang, L. Li, S. Zhao, Y. Wang and Y. Sun, *Mar. Drugs*, 2022, **20**, 375.
64 I. M. Novitskiy and A. G. Kutateladze, *Nat. Prod. Rep.*, 2022, **39**, 2003–2007.
65 M. Isaka, N. Rugseree, P. Maithip, P. Kongsaeree, S. Prabpai and Y. Thebtaranonth, *Tetrahedron*, 2005, **61**, 5577–5583.
66 M. Gao, A. E. Glenn, X. Gu, T. R. Mitchell, T. Satterlee, M. V. Duke, B. E. Scheffler and S. E. Gold, *PLoS Pathog.*, 2020, **16**, e1008595.
67 N. P. Ariantari, E. Ancheeva, M. Frank, F. Stuhldreier, D. Meier, Y. Gröner, I. Reimche, N. Teusch, S. Wesselborg, W. E. G. Müller, R. Kalscheuer, Z. Liu and P. Proksch, *RSC Adv.*, 2020, **10**, 7232–7240.
68 RDKit, https://www.rdkit.org/, accessed 14 February 2026.

